NORWEGIAN JOURNAL OF GEOLOGY
https://dx.doi.org/10.1785/njg100-2-5

GEOLOGICAL SOCIETY OF NORWAY

Evolution of metal-bearing fluids at the Nussir and Ulveryggen sediment-hosted Cu deposits, Repparfjord Tectonic Window, northern Norway

Yulia Mun[1], Sabina Strmić Palinkaš[1], Kåre Kullerud[2], Kjell S. Nilsen[3] & Andrey Bekker[4,5]

[1]*Department of Geosciences, The Arctic University of Norway, Tromsø, 9037, Norway*
[2]*Norsk Bergverksmusuem, 3602 Kongsberg, Norway*
[3]*Kjell Nilsen Geoconsulting, Landingsveien 80, 0767 Oslo, Norway*
[4]*Department of Earth and Planetary Sciences, University of California, Riverside, CA 92521, USA*
[5]*Department of Geology, University of Johannesburg, Auckland Park 2006, South Africa*

E-mail corresponding author (Yulia Mun): Yulia.mun@uit.no

Keywords:
- *Repparfjord Tectonic Window*
- *Nussir*
- *Ulveryggen*
- *Copper mineralisation*
- *Sediment-hosted mineralisation*
- *Basin evolution*
- *Fluid inclusions*
- *Stable isotopes*
- *Lithogeochemistry*

- *Electronic Supplement 1: List of samples*
- *Electronic Supplement 2: Thermometric data, type 1 fluid inclusions*
- *Electronic Supplement 3: Thermometric data, type 2 and 3 fluid inclusions*

The Palaeoproterozoic greenstone belts of Fennoscandia are metamorphosed and deformed volcanic and sedimentary rocks that formed in basins with a high base-metal ore potential. One of these, the Repparfjord Tectonic Window (RTW), is exposed in the Caledonides of northern Norway and contains several sediment-hosted Cu deposits including Nussir and Ulveryggen. The RTW is composed of mafic metavolcanic rocks (metabasalts, volcanoclastic metabreccia and metatuffite) intercalated with carbonate-siliciclastic sedimentary rocks (dolomitic marble, metasandstone to metapelite). This succession was deformed and metamorphosed up to greenschist to lower amphibolite facies during the Svecofennian Orogeny (c. 1.84 Ga). The Cu-mineralisation at the Nussir deposit is hosted by a dolomitic marble. It occurs mostly in the form of quartz-carbonate veins with chalcopyrite, bornite, chalcocite and covellite as the main ore minerals. In contrast, the Ulveryggen mineralisation is predominantly disseminated within a metasiliciclastic succession and dominated by chalcopyrite, bornite, chalcocite, covellite and neodigenite.

Mineralogical, geochemical, stable isotope and fluid-inclusion studies provide insights into the evolution of the Cu-bearing fluids. A wide range in homogenisation temperatures (135–350°C at the Nussir deposit and 102–520°C at the Ulveryggen deposit) and fluid-inclusion salinities (from 0.35 up to 36 wt.% NaCl equivalents) suggest an evolving system with brines developed by subsurface evaporite dissolution. Fluid-inclusion and Cu-sphalerite geothermometry data constrain the temperature-pressure conditions of the Cu mineralisation in the Nussir deposit at 330–340°C and 1.1–2.7 kbars. High salinities at relatively high temperatures within the ore-bearing fluids imply that Cu was transported predominantly by Cu-chloride complexes. The interaction of ore-bearing fluids with carbonate-rich host lithologies is proposed as the main mechanism for deposition of the Cu mineralisation at Nussir. In contrast, at the Ulveryggen

Received:
22. July 2019

Accepted:
11. June 2020

Published online:
13. October 2020

Mun, Y., Palinkaš, S.S., Kullerud, K., Nilsen, K.S., Neufeld, K. & Bekker, A. 2020: Evolution of metal-bearing fluids at the Nussir and Ulveryggen sediment-hosted Cu deposits, Repparfjord Tectonic Window, Northern Norway. *Norwegian Journal of Geology 100*, 202011. https://dx.doi.org/10.17850/njg100-2-5.

deposit the mineralisation was mostly controlled by dilution and cooling when ore-bearing fluids mixed with groundwaters. Locally, reaction of Cu-bearing fluids with sediment-hosted pyrite might also have triggered copper precipitation. Similar ranges of $\delta^{13}C$ (- 0.9 to + 2.9‰ V-PDB) and $\delta^{18}O$ (- 18.3 to - 15.9‰ V-PDB) values in carbonates from ore-bearing veins and underlying host dolomitic marbles reflect a carbonate rock-buffered system without a significant contribution of magmatic or hydrothermal CO^2.

Introduction

Stratiform Cu deposits contribute about 23% to the global Cu production (Singer, 1995). The supergiant deposits include the Siberian Palaeoproterozoic Kodaro–Udokan Basin, African Neoproterozoic Katanga Basin, and the northern Europe Permian Zechstein Basin (Hitzman et al., 2010). However, smaller-scale deposits are also found worldwide, like in the Neoproterozoic Zambian, DRC, and Kalahari copper-belts in Africa, Neoproterozoic Redstone Copperbelt in Canada, and Palaeoproterozoic Donchuan and Zongtiaoshan regions in China (Brown, 1971; Ripley et al., 1980; Chartrand & Brown, 1985; Selley et al., 2005; Dewaele et al., 2006; Brems et al., 2009; El Desouky et al., 2009; Sillitoe et al., 2010; Jiang et al., 2014). It is widely accepted that the stratiform Cu deposits are formed during the large-scale circulation of basinal fluids during rifting or continental collision. These fluids are capable of leaching base metals and transporting them to precipitation sites due to their moderate to high salinities and high oxidation potential. Common sources of base metals are mafic volcanic and plutonic rocks (e.g., Hitzman et al., 2005, 2010). The stratiform Cu deposits are usually associated with sediments that indicate extreme aridity and continentality, such as redbeds and evaporites that are laterally and stratigraphically bordered by organic-rich and pyrite-bearing shales (e.g., Gablina & Malinovskii, 2008). The oldest stratiform Cu deposits formed at the beginning of the early Palaeoproterozoic Great Oxidation Event (GOE; Bekker, 2015) on several cratons including the southern margin of the Superior Craton, the northern part of Baltica, the Magondi Belt in Zimbabwe, the Kodaro–Udokan Basin along the southern margin of Siberia in Russia, and the Kilembe deposit on the Tanzania Craton in Uganda (Kirkham, 1989; Cox et al., 2007; Master et al., 2010). Although the Fennoscandian Shield has early Palaeoproterozoic sedimentary successions that bracket the rise of atmospheric oxygen and contain redbeds as well as sulphate and halite evaporites (e.g., Melezhik et al., 2015), Cu stratiform deposits have not been characterised in these successions in detail.

The Nussir and Ulveryggen sediment-hosted Cu deposits are located within the Repparfjord Tectonic Window (RTW), one of several exposures of the Palaeoproterozoic greenstone belts within the Scandinavian Caledonides in northern Norway (Fig. 1; Viola et al., 2008; Torgersen et al., 2015b). In general, the Palaeoproterozoic greenstone belts in northern Norway are composed of classic metavolcano-sedimentary complexes with mafic metavolcanic rocks (metamorphosed pillow lavas, volcanoclastic breccias and tuffites) at the base succeeded by carbonate-siliciclastic deposits (dolomitic marble, metasandstone, metasiltstone, and metapelite) (Torske & Bergh, 2004). These greenstone belt successions record episodic deposition over several hundred million years that corresponds to different stages in basin evolution (Nordgulen & Andresen, 2008). Later, during the Svecofennian orogeny (1.92–1.75 Ga; Pharaoh & Brewer, 1990), the whole of the Fennoscandian Shield was subjected to compression during the assembly of the Nuna/Columbia Supercontinent, resulting in the regional greenschist facies and local metamorphism of amphibolite to granulite facies, for example near the Lapland–Kola and Svecofennian orogens (Bogdanova et al., 2015, 2016).

Mining activities at the Ulveryggen deposit lasted between 1972 and 1978/1979, while the Nussir deposit was discovered in the late 1970s and has not yet been exploited. Estimated resources of Cu at the Ulveryggen deposit are 3.7 million tons at 0.8 wt.% Cu, and the Nussir area contains 5.8 million tons at 1.15 wt.% Cu with Au and Ag as by-products (Nussir ASA, 2019).

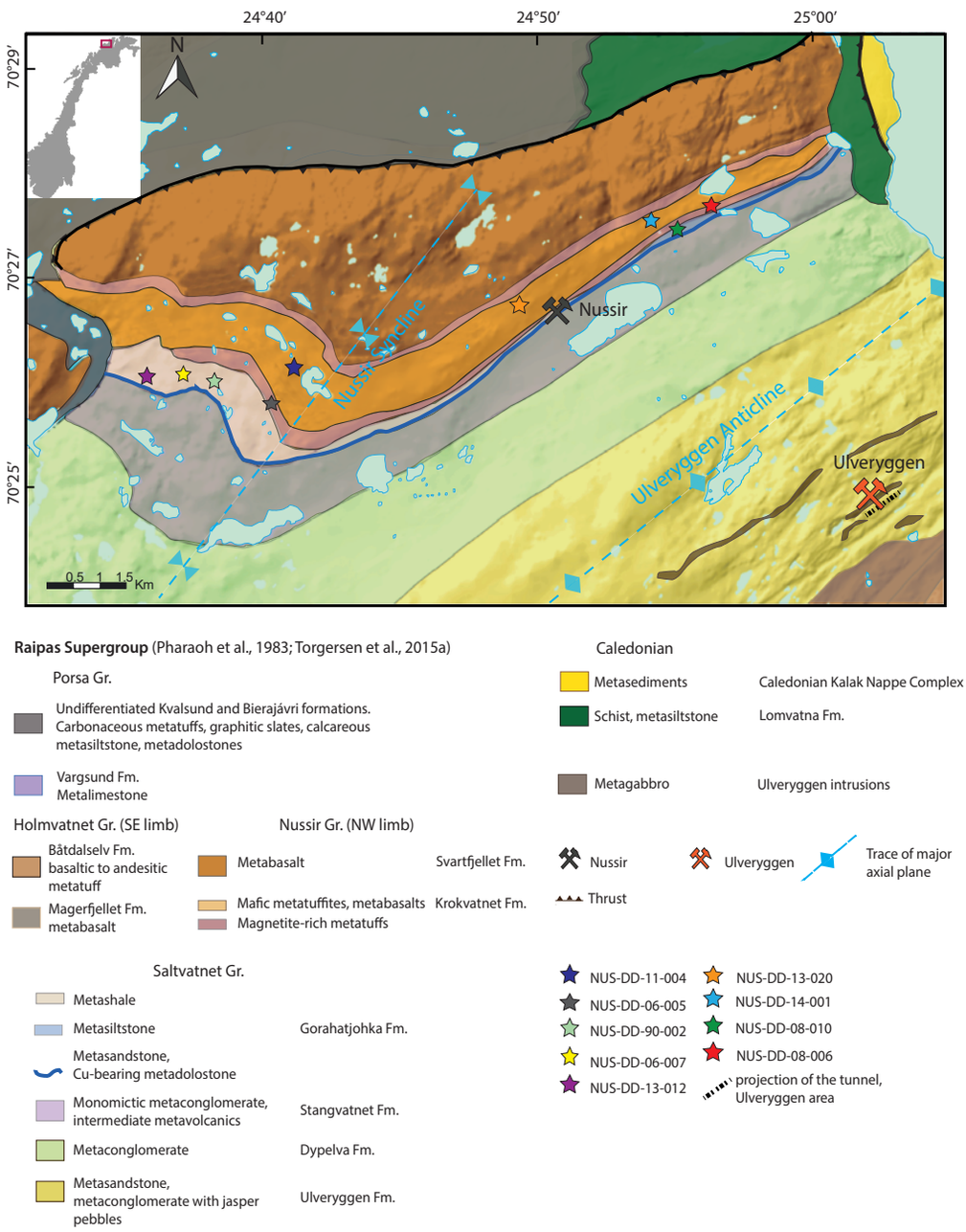

Figure 1. Simplified geological map of the Repparfjord Tectonic Window (modified after Torgersen et al., 2015a).

Despite the protracted exploration history in the RTW, the nature of ore-bearing fluids, the source of metals, and the evolution of the basin remain poorly constrained. Fabricius (1979) discussed three possible models for the genesis of the Ulveryggen mineralisation: 1) hydrothermal, with gabbroic rocks being a possible source for metals; 2) diagenetic, with detrital Cu-bearing sulphide minerals in associated siliciclastic units releasing metals; and 3) diagenetic, associated with ilmenite to rutile transformation with chalcopyrite formed as a side product ($FeTiO_3 + Cu^{2+} + 2\ H_2S = TiO_2 + CuFeS_2 + H_2O + 2\ H^+$). Stribrny (1985) suggested that the Repparfjord Copper Deposit (former name of the Ulveryggen deposit) is a marine placer deposit with a diagenetic overprint. Subsequently, Sandstad et al. (2007) inferred structural control on the Ulveryggen mineralisation, but also reported ore minerals with features consistent with both diagenetic and epigenetic modes of development. Viola et al. (2008) further reported strong structural control on Cu mineralisation hosted in mesothermal veins in the

RTW along the NE–SW, ductile, dextral-shear corridor. Perelló et al. (2015) obtained a Re–Os date for molybdenite syngenetic with the Cu-bearing mineralisation at c. 1765 Ma, which they interpreted to indicate a late syntectonic origin for the mineralisation. In contrast, Torgersen et al. (2015a) argued for progressive development of ore mineralisation under a rapidly evolving extensional to compressional regime in the basin, and related the c. 1765 Ma Re–Os molybdenite date obtained by Perelló et al. (2015) to a regional metamorphism and remobilisation event. Torgersen et al. (2015a) also inferred a multistage evolution of the mineralisation system and favoured the early diagenetic origin with the first emplacement of mineralised veins at c. 2069 ± 14 Ma (a Re–Os date on sulphides from the Porsa and Bratthammer mesothermal Cu veins associated with tholeiitic metabasalts of the Nussir Group; Torgersen et al., 2015b) and subsequent syntectonic ore remobilisation.

The focus of this study has been to constrain the origin and the nature of Cu-bearing fluids that circulated in the RTW during the Palaeoproterozoic. This study presents new petrographic and lithogeochemical data for the mineralised and barren host rocks, and mineral chemistry of the ore minerals. Petrography and microthermometry of fluid inclusions entrapped by quartz in ore-bearing veins, as well as carbon and oxygen isotope compositions of carbonates from mineralised veins and host metadolostones, were also studied and are reported here.

Geological setting

The RTW is a Palaeoproterozoic basement culmination within the Kalak Nappe Complex of the Caledonian Middle Allochthon (Fig. 1; Corfu et al., 2007; Kirkland et al., 2006; Pharaoh et al., 1983; Reitan, 1963; Viola et al., 2008). The window exposes a c. 2.1 Ga greenstone belt (Torgersen et al., 2015a) broadly correlative with the Kautokeino and Karasjok greenstone belts exposed in the Fennoscandia foreland of the Caledonides (Pharaoh et al., 1983; Siedlecka et al., 1985; Melezhik et al., 2015). The RTW consists of metasupracrustal rocks of the Raipas Supergroup, which were affected by compression during the Svecofennian Orogeny (Pharaoh et al., 1982). The compression took place in a NW direction, which resulted in greenschist to lower amphibolite-facies regional metamorphism, after c. 1.90 Ga (Bingen et al., 2015; age of foliation parallel to the gabbro body of the Rødfjellet suite). A K–Ar average age of c. 1842 Ma on amphibole possibly records the Svecofennian Orogeny (Pharaoh et al., 1982). Caledonian nappes were thrust with a SE transport direction during the Silurian (425–400 Ma) (Corfu et al., 2007; Gee et al., 2008).

The stratigraphy of the Raipas Supergroup of the RTW has been described by numerous authors (e.g., Reitan, 1963; Pharaoh et al., 1982, 1983; Pharaoh & Pearce, 1984; Viola et al., 2008; Mun, 2013) and recently revised by Torgersen et al. (2015a) (Fig. 1). Four lithological successions, from the oldest to the youngest are: (1) the Saltvannet Group, a volcano-sedimentary sequence cropping out in the hinge of the Ulveryggen anticline (Fig. 1); the subaerial metavolcanic rocks of (2) the Holmvatnet and (3) the Nussir groups, represented by tholeiitic metabasalt lavas and metatuffs cropping out in the southeastern and northwestern limbs of the Ulveryggen anticline, respectively; (4) the Porsa Group including the Vargsund, Kvalsund, and Bierajávri formations (Fig. 1) composed of carbonate-rich rocks, with locally developed stromatolites, quartz metasandstones, metatuffs, schists and slates, thrust in a SE direction along the Kvenklubben Fault upon the Nussir Group sedimentary rocks at the northwestern edge of the RTW (Torgersen & Viola, 2014; Torgersen et al., 2014). In some places, the basal polymictic metaconglomerate indicates erosion of the Nussir Group prior to deposition of the Porsa Group sediments (Pharaoh et al., 1983; Torgersen et al., 2015a). The Saltvannet Group has been of major economic interest in the RTW, where it hosts the Cu-deposits of Ulveryggen and Nussir (Fig. 1). The group can be further subdivided into four formations (listed from the oldest to the youngest): the Ulveryggen, Djupelv, Stangvatnet and Gorahatjohka formations (Fig. 1; Torgersen et al., 2015a).

In the central to southern part of the RTW, the supracrustal rocks are intruded by numerous ultramafic to mafic intrusions of Svecofennian age. The Rødfjellet (Raudfjellet) Suite of gabbro-peridotite-pyroxenite-norite composition forms sheets or podiform intrusions (Reitan, 1963; Pharaoh et al., 1983; Pharaoh, 1985; Jensen, 1996; Viola et al., 2008), and the Kvitfjell Suite consists of tonalites and trondhjemites in the southwestern part of the RTW. All intrusive rocks were subjected to low-grade metamorphism similar to that of their host rocks. The RTW is cross-cut by a number of tectonic dislocations such as the Kvenklubben Fault in the northwest, the Skifergangen shear zone, the Porsavannet Fault and the Markopp Fault, as well as thrusts with top-to-the-SE transport direction which are common in the region (Torgersen et al., 2015a) but are outside of the area shown on Fig. 1.

Geochronological age constraints for deposition of the Raipas Supergroup come from U–Pb zircon dating of mafic tuffites from the Krokvatnet Formation of the Nussir Group, which yielded the youngest mode of zircon ages at 2073.1 + 23.2 / - 12.4 Ma (Perelló et al., 2015). Bingen et al. (2015) obtained a SIMS $^{207}Pb/^{206}Pb$ zircon date of 1903 ± 18 Ma for a gabbro of the Rødfjellet mafic to ultramafic suite that intrudes the Doggejohka Formation which could be correlative to either the Saltvannet Group or the Holmvatnet Group. Bingen et al. (2015) interpreted this date as a crystallisation age for the gabbro and minimum depositional age for the Doggejohka Formation. Bingen et al. (2015) also obtained a ^{40}Ar - ^{39}Ar age of 1743 ± 4 Ma for biotite overgrowing hornblende in the same intrusion, which they related to either a regional metamorphic event or cooling and biotite closure in its aftermath.

The Ulveryggen deposit is predominantly hosted by coarse-grained, braided fluvial arkosic metasandstones of the Ulveryggen Formation. The Ulveryggen Formation is overlain by metaconglomerates of the Dypelva and Stangvatnet formations. The metaconglomerate grades stratigraphically upward from a green-coloured variety, bearing pebbles of metabasalt and metatuffite with rare pebbles of metajasper, quartzite and metadolostone, to a purple polymictic metaconglomerate with metadacite clasts (Pharaoh et al., 1983; Torgersen et al., 2015a). The Gorahatjohka Formation, which was previously described as a part of the Stangvatnet Formation (Pharaoh et al., 1983; Viola et al., 2008), hosts the Nussir Cu deposit and is composed of volcanoclastic metasiltstones and dolomitic marble (Torgersen et al., 2015a).

Sediment-hosted Cu mineralisation

The Nussir deposit

The Cu mineralisation in the Nussir deposit is mostly hosted in a dolomitic marble horizon that is intercalated with metapelites in the middle part of the Gorahatjohka Formation (Figs. 1, 2 & 3). The Gorahatjohka Formation was subdivided by Torgersen et al. (2015a) into three members of which the lower and middle are mineralised. Their thickness does not exceed 5 m and they can be followed for several kilometres from northeast to west (Fig. 1). The Gorahatjohka Formation is underlain by metaconglomerates of the Stangvatnet Formation. Within the dolomitic interval, green to light-grey dolomitic marble layers intercalate with 2 to 5 cm-thick beds of metapelite, metadolobreccia, metasandstone and metaconglomerate. The green colour of the host rocks is related to the ubiquitously developed chlorite, muscovite and sericite. The Cu-mineralised horizon is approximately 3 m thick in the NS-DD-08-006 drillcore at a depth of around 210 m. The Cu mineralisation in dolomitic marble, metasandstone and metasiltstone forms irregular masses and fine-grained aggregates within thin carbonate and quartz veins, as it occurs in disseminated form (Fig. 4, Sandstad, 2010; Perelló et al., 2015; Torgersen et al., 2015a).

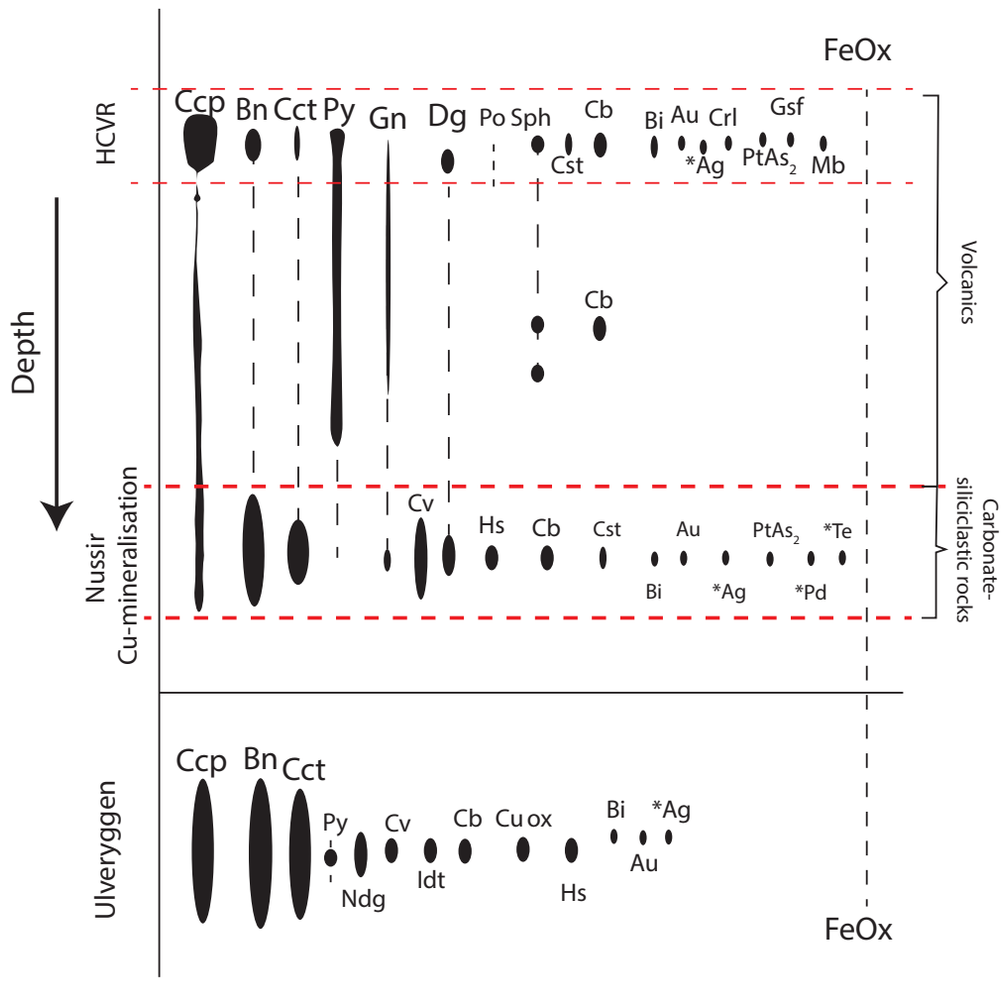

*Figure 2. Schematic diagram illustrating the modal distribution of ore minerals in the Nussir and Ulveryggen deposits. The figure is compiled from Stribrny (1985), Sandstad (2010), Mun (2013) and results of this study. HCVR – highly carbonated volcanic rocks; *Ag – different Ag-bearing minerals including hessite, naumannite, bohdanowiczite, amalgam, undifferentiated phases, Au – different Au-bearing minerals including electrum, bogdanovite, sylvanite, Bi – native bismuth, Bn – bornite, Cb – cobaltite, Ccp – chalcopyrite, Cct – chalcocite, Crl – carolyte, Cst – clausthalite, Cu ox – Cu oxides, Cv – covelline, Dg – digenite, Fe-oxides – iron-oxides, Gn – galena, Gsf – gersdorffite, Hs – hessite, Idt – idaite, Mb – molybdenite, Ndg – neodigenite, PbSe – lead selenide, *Pd – undifferentiated Pd phases including isomertierite, Po – pyrrhotite, $PtAs_2$ – sperrylite, Py – pyrite, Sph – sphalerite, *Te – Te-bearing phases with Pd and Ag.*

Locally, the mineralisation extends to the overlying metavolcanic rocks of the Holmvatnet and Nussir groups (Figs. 1, 2 & 3; Torgersen et al., 2015a). The Cu mineralisation within metavolcanic rocks is associated with extensive carbonatisation and chloritisation (Figs. 2 & 3). Mineralisation occurs in two forms: in quartz-carbonate veins and veinlets, and in disseminated form filling the space between grains and rock fragments in the host rocks. Small, nest-shaped accumulations and rare disseminations have been found in the overlying metatuffs and intercalated metasandstones (Fig. 3).

The ore mineralisation (Fig. 2) consists of chalcopyrite, bornite, chalcocite and covellite intergrown with pyrite, galena, sphalerite, and Ag and Bi minerals (e.g., Sandstad, 2010; Mun, 2013, Perelló et al., 2015). In metatuffites, chalcopyrite and pyrite dominate, while carbonates contain mostly bornite, chalcocite and, to lesser extent, chalcopyrite. Cinnabar (Hg), native Au, electrum (Au, Ag), amalgam (Ag), Au–Ag-tellurides, sperrylite ($PtAs_2$), bohdanowiczite ($AgBiSe_2$), naumannite (Ag_2Se), native Bi and wittichinite (Cu_3BiS_3) are found in association with the Cu mineralisation (Sandstad, 2010). Fig. 3 schematically shows the paragenetic sequence of the Nussir ore field.

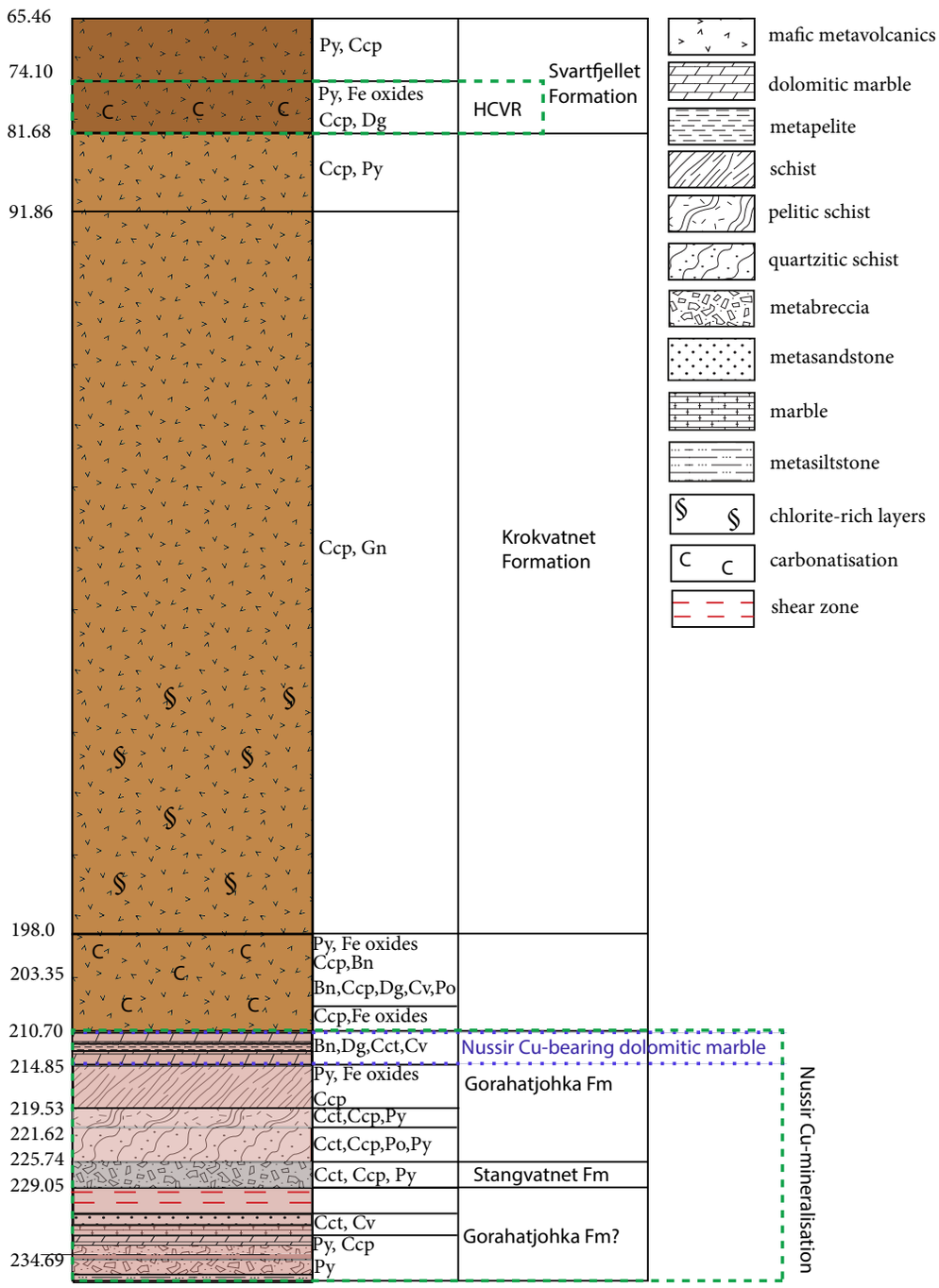

Figure 3. Lithological column for the drillhole NS-DD-08-006 through the Nussir deposit (coordinates: 7819891.79N, 395912.56E). The colours correspond to the legend in Fig. 1. Ore mineral abbreviations follow Fig. 2.

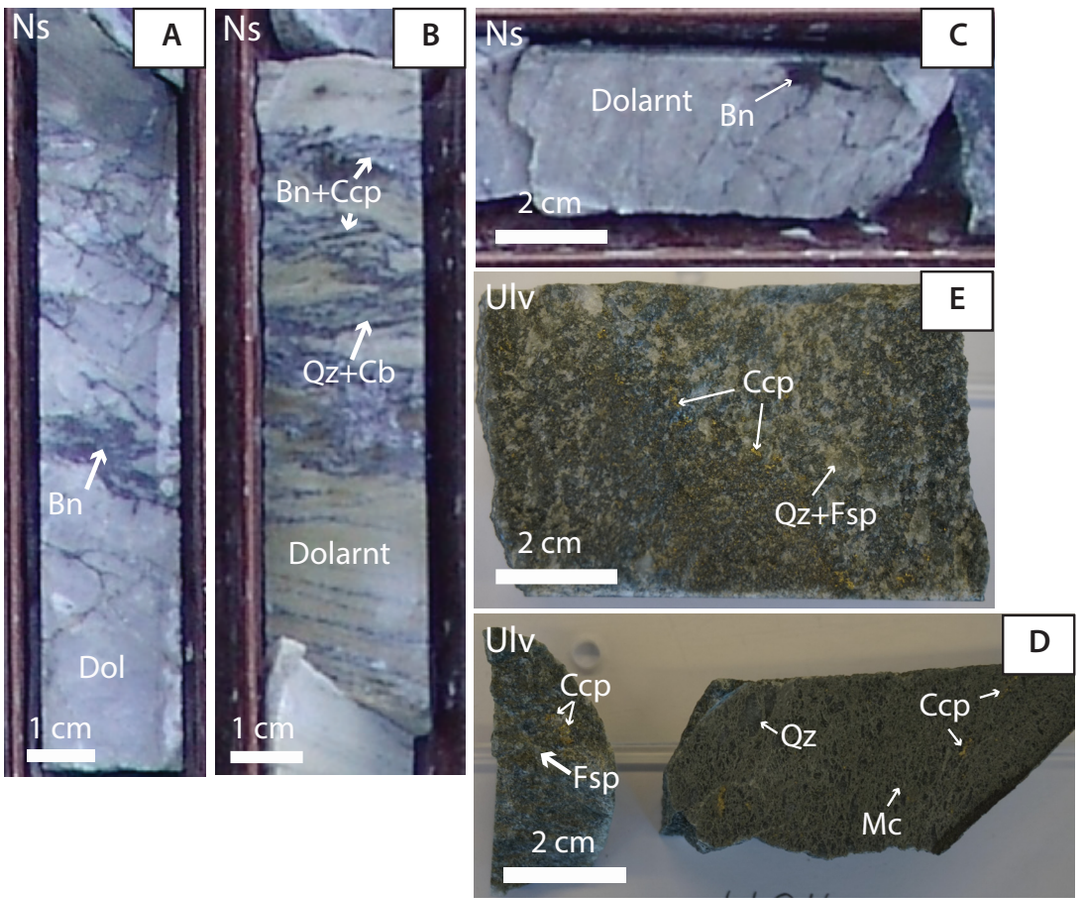

Figure 4. Photographs of core samples from the Nussir deposit (drillhole NUS-DD-06-007, 20-30 m interval) and the Ulveryggen deposit (drillhole US-004-10). (A–C) the Nussir deposit (Ns) Cu-bearing dolomitic marble (Dol) and metadoloarenite (Dolarnt). The dolomitic marble and metadoloarenite are hydrothermally altered and have quartz (Qz) - carbonate (Cb) veins enriched in bornite (Bn) and chalcopyrite (Ccp). (D–E) the Ulveryggen deposit (Ulv) mineralised arkosic metasandstone at 48.5 m and 45.16 m depth, respectively. The mineralisation is disseminated within white mica (Mc) between Qz and feldspar (Fsp) grains. Bn – bornite, Cb – carbonate, Ccp – chalcopyrite, Dol – dolomitic marble, Dolarnt – metadoloarenite, Fsp – feldspar, Mc – mica, Ns – Nussir, Qz – quartz, Ulv – Ulveryggen.

The Ulveryggen deposit

The Cu mineralisation in the Ulveryggen deposit is hosted by the metasedimentary complex, comprising fine-grained, polymictic, reddish arkosic to quartz metasandstone, conglomeratic metasandstone and metasiltstone containing grains of quartz, feldspar, chlorite, muscovite, biotite and epidote (Stribrny, 1985). The mineralisation is disseminated and, to a lesser extent, occurs in veins and veinlets controlled by tectonic structure (Sandstad et al., 2007; Perelló et al., 2015). The disseminated mineralisation is also controlled by the sediment grain size and sorting within the host sedimentary lithology. The underlying, coarse conglomeratic layers are characterised by a higher Cu grade, although the grade distribution is rather heterogeneous within the host rock (Stribrny, 1985). Fine-grained, poorly rounded, siliciclastic rock fragments range in size from 0.5 to 2 cm (Fig. 4).

The Cu mineralogy is similar to that described for the Nussir area. It consists of chalcopyrite, bornite, chalcocite and digenite in an association with pyrite and covellite. Cuprite and tenorite have also been observed (Stribrny, 1985). A wide spectrum of Fe (hematite, magnetite, maghemite, goethite and turgite) and Ti minerals (ilmenite, anatase and titanite) as well as wittichenite, renierite and idaite have been found in minor quantities (Stribrny, 1985).

Samples and methods

Samples were collected from 9 drillcores from the Nussir deposit (Fig. 1, Electronic Supplement 1) and 5 drillcores from the Ulveryggen deposit. The sampled drillcores from the Ulveryggen deposit are located close to the tunnel shown on Fig. 1. Samples were collected from 1) barren host rocks (i.e., volcanic and sedimentary rocks), and 2) Cu-mineralised rocks including hydrothermal veins. The drillcore NS-DD-08-006 from the Nussir deposit was sampled in order to characterise the stratigraphic section in detail.

Whole-rock geochemical analyses were performed at Activation Laboratories (Actlabs, Canada). Lithium metaborate/tetraborate fusion was used as a dissolution method to ensure total acid dissolution of minerals such as zircon, monazite and xenotime prior to analysis using ICP-OES and ICP-MS to determine major and trace element contents. Loss-on-ignition (LOI) upon combustion at 450°C for 4 hours is reported. Only total iron content was determined. Replicate analyses of samples and certified reference materials were used to assure the precision and accuracy of data. Repeated analyses of standards reproduced certified values within 1% accuracy for major elements and 20 ppm for trace elements. The mean precision of analyses is within 1% for major elements and within 30 ppm for trace elements.

Chemical analyses of individual ore minerals were performed using a Cameca SX 100 electron microprobe at the Department of Geosciences at the University of Oslo; a Jeol JXA 8800R Superprobe at the Institute of Geology and Geophysics of the Republic of Uzbekistan; a Zeiss Merlin Compact VP field emission scanning electron microscope (SEM) equipped with Energy-dispersive X-ray spectrometer (EDS) and wavelength-dispersive spectrometer (WDS) at UiT The Arctic University of Norway; and a NovaNanoSEM 450 at the University of California, Riverside. The analyses performed with the Cameca SX 100 were carried out at 15 kV accelerating voltage, 15 nA beam current, focused beam, 10 s counting time on a peak, and 10 s background counting time (5 s at each shoulder of the peak); no special subtraction method was applied. Standardisation was performed on synthetic minerals (As: gallium arsenide), metals (Fe, Co, Cu, Ni, Ag and Au), and on natural minerals (Zn, S: sphalerite, Pb: galena). Due to the drift of S Kα position in the WDS spectrometer analyses, analysed sulphur content could be erroneously low. To rectify this, S is frequently calibrated and the data are corrected for this drift. There was no correction applied for Mo overlap on S. The position of analytical spots was guided by the built-in optical system and pre-collected backscattered electron images. The analyses obtained with the Jeol Superprobe were carried out at 20 kV accelerating voltage, under a high-vacuum regime. The NovaNanoSEM 450 was set in a high vacuum regime at 20 kV accelerating voltage, 10 s counting time, and with an aperture of 60 µm. The Zeiss Merlin SEM field emission microscope was run in a high vacuum regime (chamber pressure $<1 \times 10^{-5}$ mbar) at 20 kV accelerating voltage, 20 s counting time, and with an aperture of 60 µm. EDS analysis automatically uses a standard for elemental content calculation with the Aztec program. The calibration was performed regularly.

Carbon and oxygen isotope analyses of carbonates were performed at UiT The Arctic University of Norway and at the SIFIR laboratory of the Department of Geological Sciences, University of Manitoba, Canada. At UiT, 50–150 µg of microdrilled carbonate powder was loaded into sealed reaction vessels, then flushed with helium gas, and reacted at 50°C with phosphoric acid over more than 2 hours. The evolved carbon dioxide was sampled using a Thermo Fisher Gasbench II and isotope ratios were measured in a continuous flow mode using a Thermo Fisher MAT253 isotope-ratio mass-spectrometer. All carbon and oxygen isotope data for carbonates in this study are reported in the delta (δ) notation as per mil (‰) deviation relative to the Vienna Pee Dee Belemnite (V-PDB). The analytical reproducibility was better than ± 0.1‰ for $\delta^{13}C$ and $\delta^{18}O$. The UiT mass-spec laboratory used three in-house calibration standards calibrated with international NBS18, NBS19 and LSVEC standards. Quality control was performed by the replicate runs of the reference samples.

At the SIFIR laboratory, carbonates were microdrilled with diamond drill bits 1 mm in diameter from the least altered (i.e., lacking veins, discoloration, weathering rinds, and silicification) and finest-grained portions of polished thick-sections, the slabs were subsequently stained to determine carbonate mineralogy. Carbonate powders were reacted at 70°C with anhydrous phosphoric acid using a GasBench II carbonate device and delivered in a stream of high-purity He to a Thermo Fisher Delta V Plus isotope ratio mass spectrometer via an open-split interface (ConFlo IV, Thermo Fisher). Calibration was performed by analysing two international calcite standards (NBS-18 and NBS-19) at the beginning, middle and end of each run. A calibration line was calculated by least squares linear regression using the known and measured isotope values of the calibration standards. To check the quality of the analysis performance, one calibrated internal calcite standard (CHI, $\delta^{13}C$ = - 8.01‰ V-PDB and $\delta^{18}O$ = - 11.67‰ V-PDB) and one calibrated internal dolomite standard (Tytyri, $\delta^{13}C$ = + 0.78‰ V-PDB and $\delta^{18}O$ = - 7.07‰ V-PDB) were analysed together with unknown samples. Replicate analyses of internal standards yielded the results of $\delta^{13}C$ = - 7.98 ± 0.08‰ and $\delta^{18}O$ = - 11.63 ± 0.14‰ (n = 23) for CHI, and $\delta^{13}C$ = + 0.74 ± 0.09‰ and $\delta^{18}O$ = - 6.02 ± 0.15‰ (n = 17) for Tytyri. Correction using the known oxygen isotope value for the Tytyri dolomite standard was performed for $\delta^{18}O$ values of dolomite samples.

Petrographic and microthermometric studies of fluid inclusions were performed at UiT. Double-polished, 0.1 to 0.3 mm-thick, quartz wafers were prepared, and measurements were carried out on a Linkam THMS 600 stage mounted on an Olympus BX 2 microscope using 10× and 50× Olympus long-working distance objectives. Two synthetic fluid-inclusion standards (SYN FLINC; pure H_2O and mixed H_2O–CO_2) were used to calibrate the equipment. The precision of the system was ± 2.0°C for homogenisation temperatures, and ± 0.2°C in the temperature range between - 60°C and + 10°C. The apparent salinity of two-phase (L + V) inclusions was calculated from the final ice melting temperature and the salinity of three-phase (L + V + S) inclusions was calculated from the final halite melting temperature. In both cases the equation of Bodnar (1993) and Bodnar & Vityk (1994) was applied. The computer package FLUIDS (Bakker, 2003; Bakker & Brown, 2003) was used to calculate fluid properties, including the bulk density. The fluid-inclusion bulk density and isochores were calculated according to the equation of state published by Zhang & Frantz (1987).

After measuring microthermometric parameters of about eighty fluid inclusions from Nussir samples NS-51 (a–k), NS-52 (a–c) and NS-53 (eutectic temperature, last melting temperature of ice and/or halite, and total homogenisation temperature), fluid inclusions were decrepitated by quick heating of the samples (100°C per min) up to 600°C and by keeping the samples at this temperature for 30 minutes, following the procedure described by Kontak (2004). The samples were subsequently inspected under reflected light for the presence of evaporate mounds and then placed on carbon tape for analysis on a SEM using the EDS detector at UiT The Arctic University of Norway.

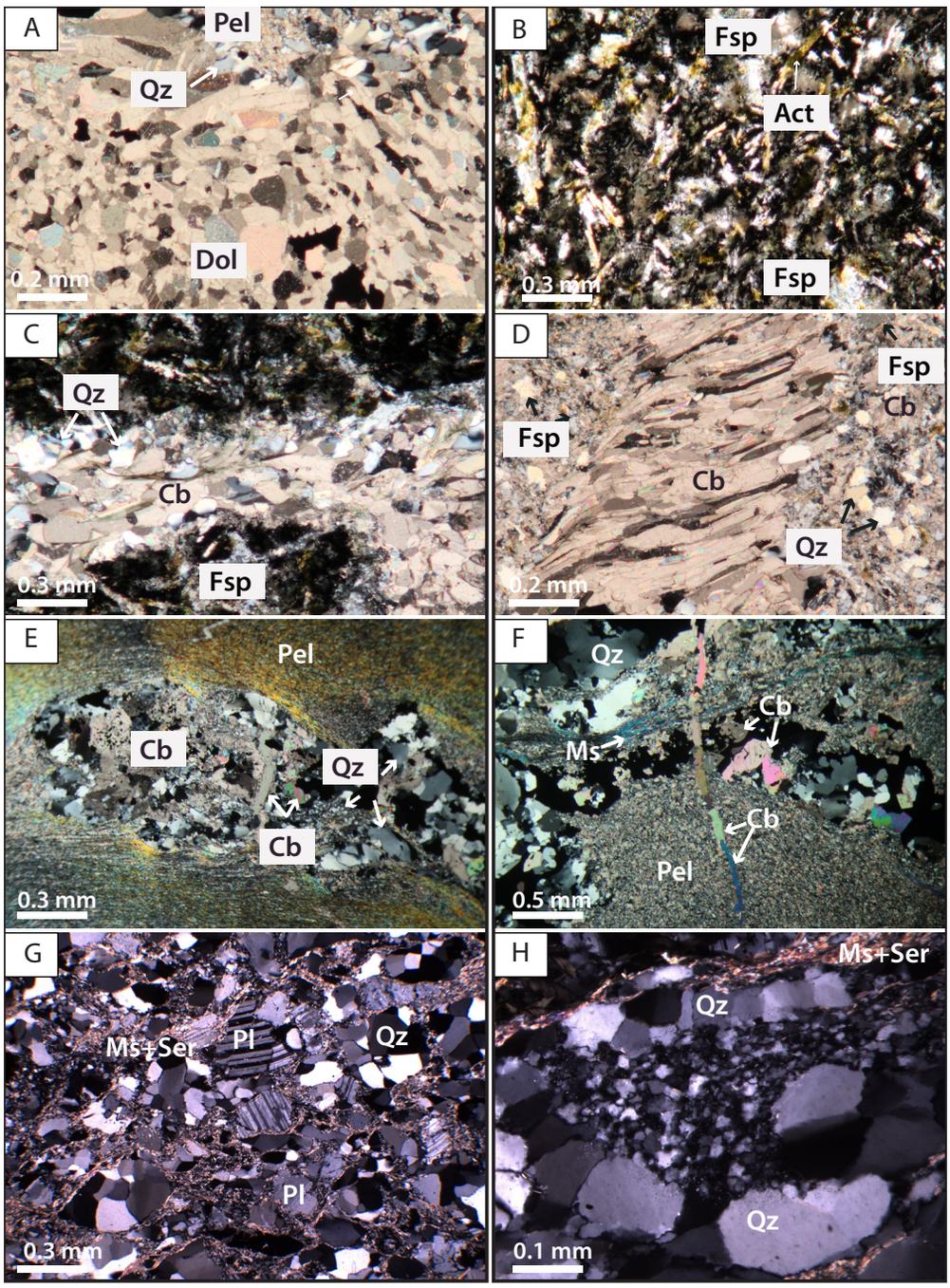

Figure 5. Photomicrographs taken in cross-polarised light of typical host rocks and veining at the Nussir and Ulveryggen deposits: (A) metadolostone (Dol) with rip-up clast of metapelite (Pel) and quartz vein (Qz); NS-16 sample; (B) metavolcanics with actinolite (Act) and feldspar (Fsp) crystals; NS-10 sample; (C) quartz-carbonate vein in metavolcanics; NS-10 sample; (D) deformed carbonate vein in carbonaceous metasandstone; NS-14 sample; (E) sigmoidally shaped quartz-carbonate vein with ore minerals (black) in metapelite (Pel); sample NS-1a; (F) carbonate vein cross-cutting metapelite (Pel), quartz, carbonate and ore minerals (black). Secondary muscovite (Ms) developed in the host metasiltstone; sample NS-1a; (G) metasandstone with grains of quartz and feldspar and with muscovite and sericite (Ser) along grain boundaries; sample Ulv-2; (H) cluster of recrystallised quartz from the vein in the host metasandstone; sample Ulv-4. Act – actinolite, Cb – carbonate, Dol – metadolostone, Fsp – feldspar, Ms – muscovite, Pel – metapelite, Pl – plagioclase, Qz – quartz, Ser – sericite.

Results

Petrography of the host rock

The Nussir deposit

The petrographic description of the metavolcano-sedimentary succession in the Nussir deposit (Fig. 3) is based on samples collected from the 65.64–234.69 m interval of the drillcore NS-DD-08-006 (Fig. 1). The lower part of the sequence is composed of carbonate-siliciclastic strata, whereas altered mafic metavolcanics prevail in the uppermost part. The carbonate-siliciclastic package consists of interlayered metasandstone, marble, dolomitic marble and metasiltstone with a few layers of metaconglomerate. This sequence is cut by a shear zone (Fig. 3).

In the sandstone of the Gorahatjohka Formation, the grains are composed of quartz and sericitised feldspar. Quartz grains are about 0.1 mm in diameter and are commonly rounded, but there are also angular varieties. Feldspar grains are poorly rounded and up to 100 µm in diameter. The grains are surrounded by a chlorite and muscovite matrix. Beds of schist, quartz-rich semi-pelite, metasiltstone and metabreccia alternate from 225 to 214 m depth. The quartz grains are irregular in shape and are up to 0.1 mm in diameter. The metasiltstone consists of poorly rounded quartz and feldspar grains, which are surrounded by a mica matrix. Metaconglomerate of the Goraharjohka Formation is composed of subrounded fragments of dolostones and doloarenites, which are larger than 2 cm in diameter. This sequence is overlain by dolomitic marble interlayered with metapelite (Fig. 5A), which is the ore-bearing horizon (Fig. 3). An approximately 4 m-thick layer of metabreccia, likely of the Stangvatnet Formation, is observed in the interval from 225 to 229 m depth. The breccia is composed of clasts of a microporphyric mafic rock. The clasts are bigger than 2 cm in diameter and are poorly rounded.

Mafic metavolcanic rocks, predominantly metatuffites, constitute an almost 150 m thickness of strata in the upper part of the section. The lower portion of the metavolcanics are intensely carbonatised and chloritised, and chlorite content decreases up-section. The metatuffite is composed of quartz, plagioclase and biotite grains in a fine-grained matrix. Quartz grains are mostly anhedral and smaller than 0.05 mm in diameter. Biotite grains have a tabular shape, commonly replaced by chlorite, and vary from 0.1 to 1 mm in size. Feldspar grains also have a tabular shape, and are generally sericitised (Fig. 5B, C). At a depth of about 81 m, metatuffite is strongly carbonatised and mineralised (the uppermost horizon is marked as highly carbonatised volcanic rocks (HCVR) in Fig. 3). The mafic metavolcanic rocks are also cross-cut by quartz-carbonate veins, but these are less abundant at this stratigraphical level than in the underlying carbonate-siliciclastic section.

In the interval between 229.64 and 231.90 m, a shear zone characterised by intensely crushed, chloritised and schistose rocks is observed. The whole stratigraphic sequence is cross-cut by mm- to cm-thick quartz-carbonate veins and veinlets (Fig. 5C–F). The main carbonate mineral in the veins and veinlets is dolomite (Fig. 5D–F). Carbonate in the early-generation veins is strongly deformed (Fig. 5D) and varies in size from 0.1 to 5 mm across. In contrast, the late-generation veins are not deformed and consist of considerably smaller crystals.

In the uppermost (28.45–28.92 m) part of the drillcore NUS-DD-06-007, deformation structures such as crenulation cleavage in mica-rich layers, sigmoidally shaped quartz and carbonate grains as well as elongated and recrystallised quartz grains in the veinlets suggest that the succession experienced compression after its deposition (Fig. 5E). Abundant chlorite and actinolite as well as sericitisation of

K-feldspar and plagioclase indicate that the rocks have undergone greenschist-facies metamorphism and hydrothermal alteration (Fig. 5B, C). Other studied drillcores (DD-14-001, DD-13-012, DD-13-020, DD-90-002, NUS-DD-11-004 and NUS-06-005; Fig. 1) show a similar distribution of lithologies to those described above for the drillcore NS-DD-08-006.

Ulveryggen deposit

The Ulveryggen deposit is hosted in the Ulveryggen Formation (Fig. 1) and it is stratigraphically below the Nussir deposit. The Ulveryggen mineralisation is hosted by massive arkosic metasandstone interlayered with metaconglomerates (Fig. 5G, H). The main components of the metasandstone are quartz and feldspars. A muscovite matrix surrounds the grains, and the size of the quartz grains ranges from <0.03 mm up to ~0.2 mm in diameter. The mineralisation is predominantly disseminated, filling space between plagioclase and quartz grains. Rare quartz veinlets, up to 1 cm in length, with aggregates of recrystallised quartz and carbonates have also been observed. Quartz crystals within the veinlets do not exceed 20 µm in size (Fig. 5H).

Whole-rock geochemistry

Whole-rock geochemical analyses were performed on the mineralised and nonmineralised volcanic rocks as well as on sedimentary rocks from the Nussir and Ulveryggen deposits (Tables 1–3). The mineralised and nonmineralised volcanic rocks at Nussir show overlapping SiO_2 concentrations (49.08 ± 4.76 and 50.31 ± 6.82 wt.%, respectively). In contrast, the mineralised volcanics are enriched in CaO (6.49 ± 4.21 wt.%) and Na_2O (4.23 ± 1.36 wt.%), but depleted in K_2O (0.78 ± 0.44 wt.%) with respect to nonmineralised equivalents (4.95 ± 2.45, 2.61 ± 1.47 and 1.67 ± 0.23 wt.%, respectively; Table 1).

Trace element contents in mineralised and nonmineralised volcanic rocks (Table 1) show significant variation. Cu content ranges from the background level reported for mafic volcanics (Engel et al., 1965; Doe, 1994) in nonmineralised rocks up to about 8600 ppm in mineralised volcanics. Zinc and Ni show slightly elevated concentrations relative to the average mafic volcanic rock (Gale et al., 2013), but without significant difference between nonmineralised and mineralised rocks. Zinc content varies from less than 30 ppm up to 200 ppm in nonmineralised rocks, and mineralised rocks contain 30 to 210 ppm of Zn. Nickel content is higher, up to 700 ppm, in rocks with lower Cu contents, while in Cu-rich volcanic rocks the maximum Ni content is 280 ppm.

Major element contents in carbonate-siliciclastic rocks from the Nussir deposit, represented predominantly by intercalations of dolomitic marble with metapelite, metasiltstone and metasandstone, show a wide range (Table 2). CaO content varies from 0.75 to 35.48 wt.%, while Na^2O content spans from 0.01 to 3.26 wt.%. A significant range is also observed for K_2O and MgO contents, from 0.02 up to 6.70 wt.% and from 0.38 to 12.89 wt.%, respectively.

The whole-rock data for the mineralised rocks, predominantly arkosic metasandstones, from the Ulveryggen deposit are listed in Table 3. They show an average content of 77.96 ± 2.74 wt.% SiO_2, 1.45 ± 0.57 wt.% MgO, 2.51 ± 0.73 wt.% Na_2O and 0.13 ± 0.07 wt.% CaO. The average contents of Cu, Zn and Co are 7045 ± 2643.4, 25 ± 20 and 11.63 ± 3.53 ppm, respectively.

Table 1. Whole-rock data for basaltic andesites and tuffs from the Nussir deposit.Whole-rock data for basaltic andesites and tuffs from the Nussir deposit.

Sample number		NS-6	NS-13	NS-36	NS-14			NS-10	NS-44	NS-33	NS-8	NS-12	NS-42	NS-45	NS-41	NS-43	NS-34		
Major oxides, %	LD	non-min	non-min	non-min	non-min	MV	SD	low-min	low-min	low-min	min	min	min	min	min	min	min	MV	SD
Al_2O_3	0.01	14.65	11.45	15.88	10.91	13.22	2.10	12.50	13.59	14.32	13.99	14.45	9.11	11.41	13.46	12.68	11.20	12.67	1.60
CaO	0.01	1.77	5.10	4.30	8.62	4.95	2.45	7.06	4.56	5.58	4.26	2.01	15.17	11.22	2.08	2.61	10.39	6.49	4.21
Fe_2O_3(T)	0.01	13.71	13.60	18.38	4.97	12.67	4.84	16.85	15.13	15.30	13.80	15.66	7.05	12.42	16.54	13.27	14.86	14.09	2.69
K_2O	0.01	1.53	1.59	1.49	2.05	1.67	0.23	0.83	0.45	1.01	0.73	1.81	1.08	0.44	0.36	0.25	0.87	0.78	0.44
MgO	0.01	6.20	13.17	5.10	1.55	6.51	4.21	3.68	4.69	4.65	2.87	4.36	6.37	3.96	2.30	7.71	3.51	4.41	1.52
MnO	0.001	0.171	0.231	0.260	0.212	0.219	0.032	0.196	0.192	0.222	0.131	0.111	0.332	0.301	0.067	0.155	0.244	0.195	0.079
Na_2O	0.01	2.91	0.13	3.88	3.53	2.61	1.47	4.29	5.41	4.34	5.61	3.87	1.18	4.58	6.26	3.14	3.60	4.23	1.36
P_2O_5	0.01	0.15	0.20	0.24	0.15	0.19	0.04	0.15	0.30	0.34	0.24	0.22	0.14	0.26	0.11	0.16	0.32	0.22	0.08
SiO_2	0.01	54.69	42.60	44.82	59.11	50.31	6.82	45.04	51.41	47.45	52.53	53.01	44.72	45.33	56.32	54.02	41.01	49.08	4.76
TiO_2	0.001	1.457	1.576	3.196	0.656	1.721	0.922	1.918	2.350	3.091	1.834	2.023	0.791	2.095	1.434	1.568	2.107	1.921	0.572
LOI		3.75	8.98	3.33	7.76			5.97	2.37	2.53	3.70	2.84	14.34	7.33	1.62	5.11	9.36		
Total		101.00	98.63	100.90	99.52			98.50	100.50	98.82	99.69	100.40	100.30	99.36	100.60	100.70	97.47		

Trace elements, ppm																			
Ag	0.5	0.8	LLD	1.5	0.5	0.7	0.5	LLD	LLD	1.7	LLD	0.7	LLD	LLD	1.0	1.1	1.1	0.6	0.6
As	5	LLD	LLD	LLD	LLD			LLD	LLD	LLD	LLD	LLD	LLD	LLD	LLD	LLD	24	2	7
Ba	3	328	865	409	1126	682	328	185	137	295	207	381	140	167	53	43	256	186	99
Be	1	2	LLD	2	LLD	1	1	1	2	2	1	2	LLD	1	1	1	2	1	1
Bi	0.4	LLD	LLD	LLD	LLD			LLD	0.0	LLD	LLD	LLD	LLD	LLD	4.9	2.7	LLD	0.8	1.6
Co	1	72	74	49	14	52	24	36	48	41	40	48	51	39	29	61	52	45	9
Cr	20	760	1540	150	250	675	550	70	160	150	540	720	630	250	520	240	160	344	222
Cs	0.5	1.6	3.5	3.3	2.0	2.6	0.8	1.7	LLD	1.9	1.0	1.6	1.3	LLD	0.7	0.5	1.5	1.0	0.7
Cu	10	10	LLD	10	50	18	19	80	110	120	230	280	620	1190	2520	3700	8610	1746	2562
Ga	1	23	19	27	11	20	6	20	21	22	20	25	15	17	15	19	16	19	3
Ge	1	3	2	LLD	1	2	1	2	1	1	2	3	1	1	2	2	LLD	2	1
Hf	0.2	4.8	3.2	6.2	5.4	4.9	1.1	2.7	3.9	6.2	3.7	4.4	2.0	3.3	5.7	5.1	3.8	4.1	1.2
In	0.2	0.2	LLD	LLD	LLD	0.1	0.1	LLD	LLD	LLD	LLD	LLD	LLD	LLD	LLD	LLD	0.2	0.0	0.1
Mo	2	LLD	LLD	LLD	LLD			LLD	LLD	LLD	LLD	LLD	LLD	3	22	LLD	LLD	3	7
Nb	1	11	7	19	6	11	5	6	13	19	11	12	4	12	13	14	15	12	4

Ni	20	360	700	110	30	300	261	50	110	90	180	250	280	160	80	250	40	149	84
Pb	5	LLD	LLD	LLD	LLD			LLD	7	LLD	LLD	LLD	LLD	13	LLD	LLD	LLD	2	4
Rb	2	50	53	36	58	49	8	27	8	22	21	58	22	6	9	6	18	20	15
Sb	0.5	LLD	LLD	LLD	LLD			LLD	LLD	LLD	LLD	LLD	LLD	LLD	LLD	LLD	LLD		
Sc	1	31	25	23	9	22	8	21	22	28	20	27	22	17	21	19	18	22	3
Sn	1	2	LLD	2	LLD	1	1	LLD	1	2	2	2	LLD	LLD	2	2	1	1	1
Sr	2	63	73	123	154	103	37	68	159	129	58	30	171	216	42	31	141	105	63
Ta	0.1	1.0	0.6	1.5	0.6	0.9	0.4	0.5	1.1	1.6	0.8	1.0	0.3	1.0	1.1	1.1	1.0	1.0	0.3
Th	0.1	4.7	2.2	4.0	5.7	4.2	1.3	2.3	3.2	3.8	2.6	3.2	2.8	2.8	4.8	4.2	2.8	3.3	0.7
Tl	0.1	0.2	0.3	0.3	0.2	0.3	0.1	LLD	LLD	LLD	LLD	0.2	0.2	LLD	LLD	LLD	2.0	0.2	0.6
U	0.1	1.1	1.0	0.9	2.1	1.3	0.5	0.6	0.8	0.9	0.5	0.7	0.6	0.6	0.9	0.9	0.5	0.7	0.2
V	5	226	219	327	83	214	87	411	319	332	213	245	193	268	246	208	225	266	65
W	1	LLD	LLD	LLD	LLD			LLD	LLD	LLD	LLD	LLD	LLD	LLD	LLD	LLD	2	0	1
Y	2	24	22	35	19	25	6	17	23	25	19	22	12	18	22	22	16	20	4
Zn	30	110	170	200	LLD	120	76	60	140	160	50	60	70	120	30	90	210	99	54
Zr	4	196	125	238	225	196	44	100	163	229	148	173	72	142	222	215	159	162	49

REE, ppm																			
Ce	0.1	51.2	28.9	75.1	35.3	47.6	17.8	23.2	75.3	60.8	46.4	46.3	23.8	70.1	53.2	40.6	28.5	46.8	17.5
Dy	0.1	5.1	4.6	8.2	3.4	5.3	1.8	3.7	4.8	5.6	4.2	4.8	2.6	3.7	4.8	4.6	3.0	4.2	0.9
Er	0.1	2.8	2.3	4.1	2.0	2.8	0.8	1.9	2.5	3.1	2.1	2.6	1.4	2.0	2.7	2.4	1.8	2.3	0.5
Eu	0.05	1.86	1.60	2.48	0.88	1.71	0.57	1.20	2.31	1.87	1.65	1.79	0.75	1.89	1.67	1.51	0.86	1.55	0.46
Gd	0.1	6.1	4.8	8.9	3.6	5.9	2.0	3.7	6.0	5.8	4.5	5.1	2.6	5.1	5.0	4.9	3.1	4.6	1.1
Ho	0.1	1.0	0.9	1.5	0.7	1.0	0.3	0.7	0.9	1.1	0.8	0.9	0.5	0.7	0.9	0.9	0.6	0.8	0.2
La	0.1	23.2	13.6	31.7	16.2	21.2	7.0	9.6	36.0	25.0	20.3	21.1	11.5	32.2	25.2	17.6	12.3	21.1	8.3
Lu	0.04	0.33	0.25	0.39	0.29	0.32	0.05	0.24	0.30	0.39	0.26	0.32	0.18	0.25	0.35	0.31	0.24	0.28	0.06
Nd	0.1	29.7	18.4	45.9	17.0	27.8	11.6	14.3	38.4	34.6	25.5	26.7	12.8	35.7	30.2	24.3	16.1	25.9	8.7
Pr	0.05	6.84	4.00	10.50	4.35	6.42	2.60	3.12	9.37	8.24	5.98	5.99	3.04	8.67	7.18	5.55	3.79	6.09	2.17
Sm	0.1	6.9	5.1	9.9	4.1	6.5	2.2	3.5	7.4	7.7	5.5	5.9	2.9	7.0	6.3	5.5	3.4	5.5	1.6
Tb	0.1	0.9	0.8	1.4	0.6	0.9	0.3	0.6	0.9	0.9	0.7	0.8	0.4	0.7	0.8	0.8	0.5	0.7	0.2
Tm	0.05	0.38	0.31	0.56	0.28	0.38	0.11	0.26	0.34	0.43	0.29	0.37	0.21	0.29	0.36	0.33	0.26	0.31	0.06
Yb	0.1	2.3	1.8	3.1	1.9	2.3	0.5	1.6	2.1	2.7	1.8	2.3	1.3	1.8	2.2	2.2	1.7	2.0	0.4

Note: LD - limit of detection; LLD - lower than limit of detection; low-min - low-mineraliSed samples, MV - mean value; non - min - nonmineralised samples; SD - standard deviation; min - mineralised

Table 2. Whole-rock data for carbonate-siliciclastic rocks from the Nussir deposit.

Sample number		NS-15	NS-18	NS-20	NS-38	NS-24	NS-32	NS-26	NS-39	NS-37	NS-40
Major oxides, %	LD	non-min	non-min	non-min	low-min	low-min	low-min	min	min	min	min
Al_2O_3	0.01	10.50	15.08	9.88	8.84	4.21	14.12	2.02	11.94	1.16	11.43
CaO	0.01	8.98	1.62	4.89	16.04	30.15	4.32	26.46	7.54	35.48	7.52
Fe_2O_3(T)	0.01	2.17	5.97	4.04	2.58	3.31	3.38	4.00	2.22	2.69	0.81
K_2O	0.01	2.02	7.59	5.66	3.62	2.31	6.26	0.53	4.82	0.02	5.42
MgO	0.01	1.30	2.25	0.92	1.85	1.43	3.80	12.89	1.98	0.68	0.38
MnO	0.001	0.216	0.054	0.123	0.316	0.754	0.190	1.567	0.153	0.495	0.156
Na_2O	0.01	3.25	0.99	1.34	0.95	0.03	1.02	0.01	1.78	0.08	2.84
P_2O_5	0.01	0.15	0.13	0.12	0.09	0.07	0.13	0.04	0.11	0.03	0.10
SiO_2	0.01	61.20	63.33	68.60	51.90	33.09	60.51	17.34	60.04	28.95	65.55
TiO_2	0.001	0.468	0.529	0.421	0.276	0.213	0.496	0.060	0.385	0.054	0.229
LOI		8.76	3.25	4.73	14.09	24.41	6.46	34.60	7.52	29.04	6.43
Total		99.02	100.80	100.70	100.60	99.97	100.70	99.52	98.49	98.68	100.90
Trace elements, ppm											
Ag	0.5	LLD	LLD	0.9	0.6	LLD	3.0	LLD	0.6	LLD	0.5
As	5	LLD	LLD	LLD	LLD	LLD	LLD	LLD	LLD	LLD	LLD
Ba	3	3512	1898	3597	1067	620	1462	34	1549	146	1974
Be	1	1	2	LLD	1	LLD	2	LLD	2	LLD	LLD
Bi	0.4	LLD	LLD	LLD	LLD	LLD	LLD	LLD	LLD	LLD	0.9
Co	1	12	20	8	15	7	15	20	15	8	3
Cr	20	250	230	330	240	150	210	50	170	150	240
Cs	0.5	1.8	4.3	1.6	2.8	1.1	7.2	1.1	2.9	LLD	0.5
Cu	10	LLD	LLD	LLD	20	30	110	250	280	650	1500
Ga	1	11	24	11	11	8	19	4	18	3	11
Ge	1	LLD	1	LLD	LLD	LLD	LLD	LLD	LLD	LLD	LLD
Hf	0.2	4.4	3.9	6.7	2.7	2.3	5.1	0.6	3.2	LLD	2.8
In	0.2	LLD	LLD	LLD	LLD	LLD	LLD	LLD	LLD	LLD	LLD
Mo	2	LLD	LLD	3	3	LLD	6	LLD	LLD	3	10
Nb	1	5	4	5	3	2	5	LLD	4	LLD	2
Ni	20	30	50	20	40	LLD	50	LLD	30	20	LLD

Pb	5	LLD	LLD	LLD	LLD	5	LLD	LLD	LLD	LLD	11
Rb	2	62	253	124	133	60	224	24	147	LLD	81
Sb	0.5	LLD	LLD	LLD	LLD	LLD	LLD	LLD	LLD	LLD	LLD
Sc	1	7	12	5	6	4	11	2	8	3	4
Sn	1	LLD	1	LLD	LLD	LLD	1	LLD	1	LLD	LLD
Sr	2	262	39	112	140	112	54	194	69	297	71
Ta	0.1	0.5	0.5	0.5	0.4	0.2	0.6	LLD	0.4	LLD	0.2
Th	0.1	5.3	7.6	6.8	4.3	3.2	7.4	1.3	7.2	LLD	1.1
Tl	0.1	0.1	0.6	0.3	0.3	0.2	0.8	0.0	0.3	LLD	0.1
U	0.1	2.2	3.8	2.8	1.8	2.7	2.3	0.7	2.1	LLD	1.8
V	5	64	146	72	48	60	82	30	65	22	27
W	1	LLD	LLD	LLD	LLD	LLD	LLD	LLD	LLD	LLD	LLD
Y	2	19	14	16	13	16	10	12	15	10	7
Zn	30	LLD	LLD	LLD	LLD	LLD	90	LLD	LLD	40	LLD
Zr	4	167	153	273	108	93	199	21	128	6	121
REE, ppm											
Ce	0.1	32.4	53.0	45.0	42.9	41.1	45.5	94.8	31.6	1.2	46.3
Dy	0.1	3.5	2.7	3.1	2.3	2.9	2.2	2.2	2.6	0.9	1.3
Er	0.1	1.9	1.4	1.8	2.1	1.9	1.3	1.0	1.8	1.7	0.8
Eu	0.05	1.1	1	1.02	0.75	0.86	0.91	1.19	0.59	0.09	0.56
Gd	0.1	3.7	2.8	3.3	2.4	3.1	2.6	4.1	2.4	0.3	1.9
Ho	0.1	0.7	0.5	0.6	0.6	0.6	0.4	0.4	0.5	0.3	0.3
La	0.1	15.1	26.0	21.4	22.3	18.3	22.7	48.0	18.1	0.6	24.3
Lu	0.04	0.22	0.2	0.28	0.56	0.29	0.25	0.11	0.27	0.52	0.13
Nd	0.1	16.6	22.7	21.4	20.5	17.4	20.4	40.5	16.5	0.7	20.6
Pr	0.05	3.96	6.09	5.5	5.31	4.6	5.43	11	4.34	0.14	5.41
Sm	0.1	3.9	4.1	4.3	3.7	3.5	3.8	7.0	3.0	0.2	3.5
Tb	0.1	0.6	0.5	0.5	0.4	0.5	0.4	0.5	0.4	<0.1	0.3
Tm	0.05	0.25	0.21	0.28	0.37	0.27	0.2	0.12	0.27	0.29	0.13
Yb	0.1	1.5	1.3	1.8	3.0	1.8	1.5	0.7	1.8	2.6	0.9

Note: LD - limit of detection; LLD - lower than limit of detection; low-min - low-mineralised samples; non-min - nonmineralised samples; MV - mean value; SD - standard deviation; min - mineralised

Table 3. Whole-rock data for siliciclastic rocks from the Ulveryggen deposit.

Sample number		YM-03	YM-08	YM-04	YM-07	YM-05	YM-02	YM-06	YM-09		
Major oxides, %	LD	min	min	min	min	min	min	min	min	MV	SD
Al_2O_3	0.01	9.68	8.40	9.04	8.82	8.41	9.67	7.11	9.89	8.88	0.86
CaO	0.01	0.30	0.11	0.08	0.07	0.11	0.10	0.14	0.10	0.13	0.07
Fe_2O_3(T)	0.01	2.92	3.15	4.02	3.05	2.75	5.65	5.32	3.22	3.76	1.06
K_2O	0.01	1.59	1.03	1.25	0.88	1.76	2.54	1.26	2.38	1.59	0.57
MgO	0.01	1.03	1.17	2.56	0.82	1.66	2.07	0.92	1.36	1.45	0.57
MnO	0.001	0.016	0.021	0.034	0.015	0.023	0.032	0.017	0.020	0.022	0.007
Na_2O	0.01	3.08	3.25	2.41	3.73	1.82	1.44	2.27	2.11	2.51	0.73
P_2O_5	0.01	0.03	0.04	0.01	LLD	0.02	0.03	0.01	LLD	0.02	0.01
SiO_2	0.01	79.03	80.30	77.16	79.11	81.22	71.73	78.52	76.60	77.96	2.74
TiO_2	0.001	0.258	0.256	0.266	0.304	0.225	0.863	0.488	0.308	0.371	0.201
LOI		1.46	1.04	1.96	1.12	1.42	2.37	0.85	1.58		
Total		99.40	98.78	98.79	97.92	99.41	96.49	96.92	97.56		
Trace elements, ppm											
Ag	0.5	LLD	LLD	LLD	LLD	LLD	LLD	0.6	LLD	0.1	0.2
As	5	LLD	LLD	LLD	LLD	LLD	LLD	LLD	LLD		
Ba	2	562	334	338	304	485	1091	468	1207	599	330
Be	1	LLD	LLD	LLD	LLD	LLD	LLD	LLD	LLD		
Bi	0.1	LLD	LLD	LLD	LLD	LLD	LLD	LLD	3.1	0.4	1.0
Co	1	9	10	15	7	11	19	10	12	12	4
Cr	20	470	540	360	440	420	1310	820	480	605	296
Cs	0.1	0.5	0.7	0.4	0.3	0.5	0.9	0.7	0.8	0.6	0.2
Cu	10	2610	4300	5470	6910	7070	>10000	>10000	>10000	7045	2643
Ga	1	10	9	11	8	10	14	8	13	10	2
Ge	0.5	1.1	0.8	0.8	0.8	0.8	1.5	0.8	1.0	1.0	0.2
Hf	0.1	1.6	2.6	3.1	2.2	1.9	4.8	4.0	2.2	2.8	1.0
In	0.1	LLD	LLD	LLD	LLD	LLD	LLD	LLD	LLD		
Mo	2	8	7	4	8	6	11	9	6	7	2
Nb	0.2	1.0	1.1	1.4	1.5	0.8	6.9	2.8	1.2	2.1	1.9
Ni	20	50	40	50	30	50	100	50	60	54	19

Pb	5	LLD	8	LLD	LLD	LLD	LLD	LLD	LLD	1	3
Rb	1	44	28	33	22	45	74	35	61	43	16
Sb	0.2	0.4	0.4	0.3	0.5	0.4	1.2	0.3	0.6	0.5	0.3
Sc	1	6	4	5	5	5	8	5	7	6	1
Sn	1	LLD	LLD	LLD	LLD	LLD	LLD	LLD	LLD		
Sr	2	56	57	52	52	53	50	38	66	53	7
Ta	0.01	0.22	0.21	0.28	0.19	0.23	0.75	0.42	0.24	0.32	0.18
Th	0.05	3.54	5.95	5.11	4.00	5.66	16.90	14.20	4.07	7.43	4.80
Tl	0.05	0.43	0.17	0.19	0.16	0.23	0.55	0.44	0.39	0.32	0.14
U	0.01	3.24	1.25	1.47	1.13	1.00	2.10	3.53	1.67	1.92	0.90
V	5	53	48	48	41	53	78	57	66	56	11
W	0.5	0.6	LLD	0.7	0.9	2.8	4.1	LLD	LLD	1.1	1.4
Y	0.5	8.9	8.5	9.6	5.6	6.8	14.5	8.9	5.9	8.6	2.6
Zn	30	LLD	30	40	LLD	LLD	40	50	40	25	20
Zr	1	64	98	120	86	73	188	159	81	109	41
REE, ppm											
Ce	0.05	12.10	36.00	47.20	19.60	25.80	44.20	26.90	22.20	29.25	11.43
Dy	0.01	1.72	1.52	1.77	1.04	1.24	2.99	1.51	1.12	1.61	0.58
Er	0.01	0.91	0.83	0.98	0.63	0.73	1.56	0.90	0.65	0.90	0.28
Eu	0.01	0.52	0.56	0.80	0.44	0.49	1.04	0.52	0.43	0.60	0.20
Gd	0.01	1.79	1.79	2.29	1.21	1.62	2.91	1.57	1.31	1.81	0.52
Ho	0.01	0.33	0.30	0.34	0.21	0.25	0.55	0.29	0.22	0.31	0.10
La	0.05	6.97	17.10	23.00	9.19	12.80	21.10	12.90	12.60	14.46	5.20
Lu	0.002	0.133	0.140	0.154	0.116	0.127	0.242	0.162	0.120	0.149	0.038
Nd	0.05	7.02	13.70	18.50	8.17	10.10	19.60	10.60	9.48	12.15	4.39
Pr	0.01	1.71	3.95	5.22	2.18	2.83	5.00	2.90	2.70	3.31	1.20
Sm	0.01	1.81	2.42	2.99	1.52	1.93	3.86	2.00	1.67	2.28	0.74
Tb	0.01	0.29	0.27	0.33	0.18	0.22	0.50	0.25	0.19	0.28	0.10
Tm	0.01	0.13	0.13	0.15	0.10	0.11	0.25	0.14	0.11	0.14	0.05
Yb	0.01	0.83	0.86	0.96	0.73	0.70	1.57	1.00	0.76	0.93	0.26

Note: LD - limit of detection; LLD - lower than limit of detection; MV - mean value; SD - standard deviation; min - mineralised

Ore mineralogy and mineral chemistry

The Nussir deposit

A range of ore minerals have been identified in the studied samples from the Nussir deposit. Copper minerals include chalcopyrite ($CuFeS_2$), bornite (Cu_5FeS_4), digenite (Cu_9S_5), chalcocite (Cu_2S) and covellite (CuS). In addition, pyrite (FeS_2), sphalerite (ZnS), galena (PbS), clausthalite (PbSe), molybdenite (MoS_2), gersdorffite (NiAsS), argentite (Ag_2S), stromeyerite (AgCuS), chlorargyrite (AgCl), amalgam, cobaltite (CoAsS), hessite (Ag_2Te) and native Bi were found (Fig. 6A–I).

The studied drillcore (NS-DD-08-006; Fig. 3) shows a gradual vertical change in the distribution of copper and associated ore minerals. Although chalcopyrite occurs throughout the entire mineralised sequence, it prevails over other Cu minerals in the upper part of the mineralised sequence. In contrast, bornite and chalcocite are more abundant in the deeper portion of the sequence.

Chalcopyrite occurs throughout the mineralised sequence and is observed predominantly in quartz-carbonate veins. In the upper part of the drillcore, chalcopyrite contains almost no inclusions with an exception of sphalerite inclusions (at 33 m depth, Fig. 6I). Sphalerite is paragenetically linked with chalcopyrite, likely being formed simultaneously under chemical equilibrium. Sphalerite ranges in grain size from 25 to 50 µm and contains 0.47 to 0.96 wt.% Cu and 0.71 to 1.18 wt.% Cd (Table 4). In the lower part (230–730 m depth), chalcopyrite usually occurs as a secondary mineral in bornite or intergrown with pyrite (Fig. 6A, H). Chalcopyrite also occurs together with galena (Fig. 6A) and cobaltite (Fig. 6E). Electron microprobe chemical analyses (EMPA) of chalcopyrite are shown in Table 4. Chalcopyrite contains minor amounts of Zn, Ag and Au.

Bornite contains trace amounts of Ni, Zn, Se, Mo, Ag, Au, Te and Hg (EMPA, Table 4). Locally, bornite contains silver with concentrations reaching up to 3.70 wt.% (for example in sample NS-4).

In the studied section (drillcore NS-DD-0608-006; Fig. 4), bornite appears below 198.0 m depth. It is nearly always altered and partly replaced by chalcopyrite, chalcocite (Fig. 6B, D, F), digenite and/or covellite. Inclusions of galena and clausthalite as well as native Bi (Fig. 6A–D, F) have been observed within bornite.

Digenite, chalcocite and covellite are usually observed as secondary minerals. Chalcocite is commonly intergrown with bornite (Fig. 6B–D, F). Chalcocite contains minor amounts of Co, Se, Mo and Hg. Minor amounts of Ag are found in chalcocite, digenite and covellite (Table 4). Chalcocite was identified in the lower part of the drillcore NUS-DD-08-006 at depths below 203 m. Covellite occurs as a secondary copper mineral replacing chalcopyrite, bornite and chalcocite.

Pyrite (Fig. 6H) has been observed throughout the studied succession. It is distributed in the matrix as single grains and is also intergrown with chalcopyrite when the latter forms rims around pyrite (Fig. 6H). Pyrite contains trace amounts of Ag and Au (Table 4).

Galena forms inclusions within bornite, chalcocite (Fig. 6A, B), and chalcopyrite and has trace concentrations of Ag, Au, Te, Co and Ni (Table 4). The grain size of galena is generally too small (2–6 µm in diameter) to avoid interference with adjacent copper minerals during analysis, which explains the relatively high content of Fe and Cu for galena crystals. Clausthalite was found in micro-inclusions within chalcocite and bornite (Fig. 6B, C, G), however the grains do not exceed 1 µm in diameter and it was not possible to perform quantitative analyses on this mineral.

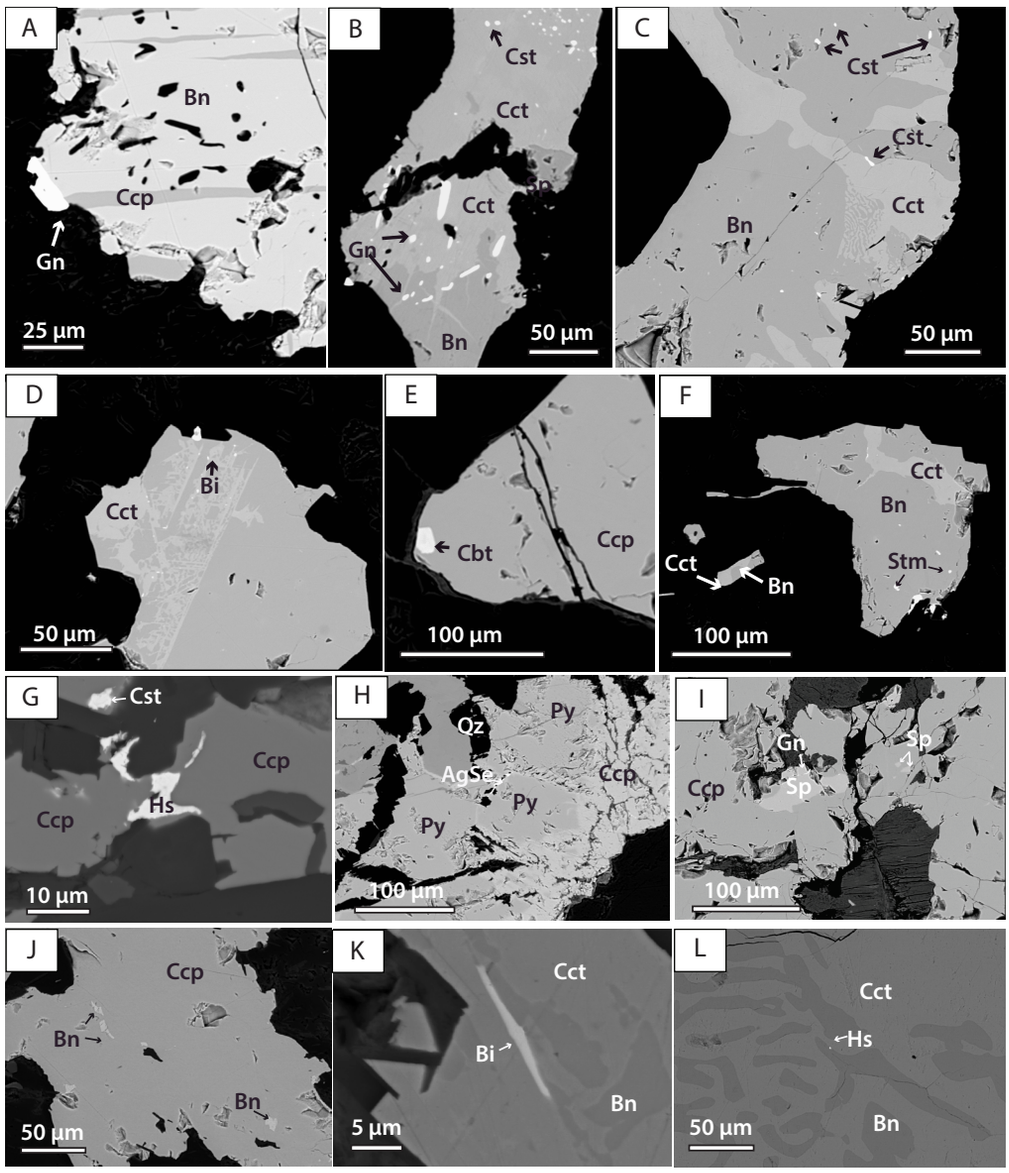

Figure 6. Backscatter electron images of mineralised samples from the Nussir and Ulveryggen deposits: (A) bornite (Bn), chalcopyrite (Ccp) and galena (Gn); sample NS-27, drillhole NUS-DD-14-001, 730 m depth; (B) bornite partially replaced by chalcocite (Cct) with inclusions of clausthalite (Cst), galena and sphalerite (Sp); sample NS-40, drillhole NUS-DD-11-004, 459.8 m depth; (C) chalcocite intergrown with bornite having small inclusions of clausthalite; sample NS-32, drill hole NUS-DD-90-002, 53 m depth; (D) native bismuth (Bi) in chalcocite-bornite aggregate; sample NS-32, drillhole NUS-DD-90-002, 53 m depth; (E) cobaltite (Cbt) inclusion in chalcopyrite; sample NS-44, drillhole NUS-06-005, 232.2 m depth; (F) stromeyerite (Stm) and AgBiS phase in bornite; sample NS-32, drillhole NUS-DD-90-002, 53 m depth; (G) inclusions of hessite (Hs) and clausthalite in chalcopyrite; sample NS-42, drillhole NUS-DD-13-020, 366 m depth; (H) chalcopyrite overgrown with pyrite (Py) crystals containing small inclusions of AgSe phase; sample NS-44, drillhole NUS-DD-06-005, 232.2 m depth; (I) inclusions of sphalerite and galena in chalcopyrite; sample NS-34, drillhole NUS-DD-11-004, 33 m depth; (J) chalcopyrite with bornite inclusions; sample Ulv-1, drillhole US-003-10, 39.1 m depth; (K) micro-inclusion of Bi-bearing mineral phase in chalcocite. Chalcocite is partly replaced by bornite; sample Ulv-12, drillhole US-015-10, 3.4 m depth; (L) vermicular intergrowth of bornite and chalcocite. Note tiny inclusion of hessite in bornite; sample Ulv-14, drillhole US-020-10, 50.1 m depth. Bi – native bismuth, Bn – bornite, Cbt – cobaltite, Ccp – chalcopyrite, Cct – chalcocite, Cst – chlausthalite, Gn – galena, Hs – hessite, Stm – stromeyerite, Qz – quartz.

Cobaltite grains, up to 10 μm in diameter, occur together with chalcopyrite (Fig. 6E) and contain trace amounts of Ni, Se, Mo, Ag, Hg and Bi (Table 4).

Silver compounds with Cl (chlorargyrite), Cu (stromeyerite), Bi (possibly matildite ($AgBiS_2$)) and argentite, together with clausthalite and native bismuth (Bi), were found predominantly at shallow depths (29 to 150 m) (Fig. 6B–D, F, H), while hessite was found below 360 m depth (Fig. 6G). Silver has been observed in its native form (amalgam) with up to 13 wt.% Hg, as argentite, chlorargyrite, stromeyerite and hessite (Table 4). Silver minerals occur as small inclusions, 2 to 20 μm in diameter, in grains of bornite, chalcocite and chalcopyrite. Chemical data for silver minerals are given in Table 4. Other minerals that are observed only rarely include gersdorffite and molybdenite (Table 4).

The Ulveryggen deposit

The ore mineralogy of the Ulveryggen deposit is similar to that of the Nussir deposit (Fig. 6J–L) and includes bornite, chalcopyrite, chalcocite, covelline, hessite, amalgam, iron oxide and an unidentified CuBiS phase. The distribution of ore minerals does not show any zoning, and minerals fill the interstitial space between quartz and feldspar grains.

Bornite and chalcocite are more abundant than chalcopyrite. Bornite replaces chalcopyrite (Fig. 6J) and chalcocite forms vermicular intergrowths with bornite (Fig. 6K, L). Bornite also contains inclusions of hessite (Fig. 6L). Chalcocite contains inclusions of native Bi (Fig. 6K). Chalcopyrite, bornite, chalcocite, pyrite and galena contain trace amounts of Au and Ag. Chemical data for selected ore minerals from the Ulveryggen deposit are given in Table 4.

Table 4. Mineral chemistry of selected ore minerals from the Nussir and Ulveryggen deposits (wt.%).

Lab	Mineral	Sample	Ag	As	Au	Ba	Bi	Cl	Co	Cu	Fe	Hg	Mo	Ni	O	Pb	S	Se	Te	Zn	Total
UiO	Ccp	NS-9	0.05	-	0.09	-	-	-	-	33.63	30.53	-	-	-	-	-	35.33	-	-	0.12	99.74
UiO	Ccp	NS-12	-	-	0.09	-	-	-	-	-	30.94	-	-	-	-	-	35.95	-	-	0.05	100.92
UiO	Ccp	NS-42	0.03	-	-	-	-	-	-	33.29	29.77	-	2.86	-	-	-	34.7	0.03	-	0.07	100.76
UiO	Bn	NS-4	3.7	-	-	-	-	-	-	58.74	10.69	-	-	-	-	-	24.97	-	-	0.08	98.2
UiO	Bn	NS-26	0.5	-	0.04	-	-	-	-	62.8	11.01	-	-	-	-	-	25.34	-	-	-	99.75
UiO	Bn	NS-27	-	-	-	-	-	-	-	60.5	14.26	0.05	-	-	-	-	26.11	0.06	0.07	0.08	101.13
UiO	Bn	NS-32	0.15	-	-	-	-	-	-	62.42	10.93	0.06	1.92	0.02	-	-	25.2	0.12	0.03	0.04	100.92
UiO	Bn	NS-40	-	-	-	-	-	-	-	62.83	10.72	-	2.18	0.04	-	-	24.95	0.42	-	0.11	101.26
UiO	Cct	NS-14	0.38	-	-	-	-	-	0.04	75.24	0.83	-	-	-	-	-	23.11	-	-	0.06	99.57
UiO	Cct	NS-32	0.22	-	-	-	-	-	0.01	78	0.19	-	1.59	0.01	-	-	20.5	0.17	-	0.14	100.83
UiO	Cct	NS-40	0.01	-	-	-	-	-	0.01	78.05	0.03	0.1	1.54	-	-	-	20.63	0.31	-	0.17	100.85
UiO	Dg	NS-16	0.17	-	-	-	-	-	-	79.21	0.12	-	-	-	-	-	20.9	-	-	0.11	100.38
UiO	Dg	NS-26	0.6	-	-	-	-	-	-	75.09	0.73	-	-	-	-	-	22.81	-	-	0.07	99.19
UiO	Cv	NS-14	0.29	-	-	-	-	-	-	62.53	11.5	-	-	-	-	-	25.98	-	-	0.07	100.36
UiO	Cv	NS-26	0.14	-	-	-	-	-	-	62.37	11.36	-	-	-	-	-	25.45	-	-	0.11	99.44
UiO	Py	NS-10	0.04	-	0.16	-	-	-	-	-	46.84	-	-	-	-	-	52.7	-	-	-	99.77
UiO	Py	NS-44	0.44	-	-	-	-	-	0.22	4.58	52.08	0.05	3.19	0.46	-	-	39.68	0.11	-	0.06	100.91

UiO	Ga	NS-4	0.02	-	0.01	-	-	-	-	0.04	0.25	-	-	-	-	86.55	13.29	-	-	-	100.1
UiO	Ga	NS-27	0.09	-	-	-	-	-	0.01	1.73	0.43	-	-	0.01	-	84.73	11.96	1.94	0.01	-	100.93
UiO	Cst	NS-32	3.99	-	-	-	-	-	-	1.28	0.42	-	0.07	-	-	68.98	0.55	25.74	-	-	101.08
UiO	Cst	NS-32	0.41	-	-	-	-	-	-	1.79	0.23	-	0.11	-	-	73.62	1.61	24.17	-	-	101.94
IGG	Mol	NS-1a	-	-	-	-	-	-	-	-	-	-	58.96	-	-	-	41.04	-	-	-	100
IGG	Gf	NS-1a	-	46.49	-	-	-	-	0.64	1.49	1.55	-	-	31.69	-	-	18.03	-	-	-	100
UiO	Cbt	NS-44	0.04	41.25	-	-	0.07	-	31.44	-	5.02	-	-	0.74	-	-	22.21	0.42	-	-	101. 0
UiO	Cbt	NS-44	0.09	41.18	-	-	0.01	-	30.97	-	4.4	0.03	1.43	0.68	-	-	21.6	0.33	-	-	100.79
UiT	Sph	NS-34	-	-	-	-	-	Cd=0.71	-	0.72	7.63	-	-	-	-	-	33.33	-	-	57.54	99.93
UiT	Sph	NS-34	-	-	-	-	-	Cd=1.18	-	0.6	6.81	-	-	-	-	-	32.93	-	-	58.74	100.26
UiT	Sph	NS-34	-	-	-	-	-	Cd=0.88	-	0.73	7.78	-	-	-	-	-	33.47	-	-	59.26	102.12
UiO	Sph	NS-44	-	-	-	-	-	-	-	0.47	6.75	-	-	-	-	-	32.84	-	-	59.93	99.99
UiO	Sph	NS-44	-	-	-	-	-	-	-	0.96	7.6	-	-	-	-	-	34.1	-	-	57.34	100
UiO	Sph	NS-44	-	-	-	-	-	-	0.17	0.73	7.05	0.07	-	0.08	-	-	32.32	0.02	-	60.20	100.66
UiT	Am	NS-27	88.2	-	-	-	-	-	-	-	-	11.8	-	-	-	-	-	-	-	-	100
UiT	Am	NS-27	86.56	-	-	-	-	-	-	-	-	13.44	-	-	-	-	-	-	-	-	100
UiT	Am	NS-4	99.3	-	-	-	-	-	-	0.283	0.11	-	-	-	-	-	0.02	-	-	-	99.72
IGG	Arg	NS-1a	87.33	-	-	-	-	-	-	0.31	-	-	-	-	-	-	12.36	-	-	-	100
IGG	Arg	NS-1a	87.02	-	-	-	-	-	-	-	-	-	-	-	-	-	12.98	-	-	-	100

IGG	Stm	NS-1a	55.14	-	-	-	-	-	-	29.33	0.41	-	-	-	-	-	15.12	-	-	-	100
IGG	Stm	NS-1a	51.26	-	-	-	-	-	-	33.39	-	-	-	-	-	-	15.35	-	-	-	100
IGG	Clag*	NS-1a	76.37	-	-	-	-	8.97	-	0.28	-	-	-	-	-	-	0.81	-	-	-	86.42
UiT	Hs	NS-43	62.57	-	-	-	-	-	-	1.8	-	-	-	-	-	-	-	-	35.63	-	100
UiT	Hs	NS-43	65.35	-	-	-	-	-	-	3.19	-	-	-	-	-	-	-	-	31.46	-	100
UiT	Hs	NS-43	58.46	-	-	-	-	-	-	1.95	-	-	-	-	-	-	-	-	39.59	-	100
UiT	Hs	NS-43	60.09	-	-	-	-	-	-	3.58	-	-	-	-	-	-	-	-	36.33	-	100
UiT	Hs	NS-43	61.1	-	-	-	-	-	-	3.18	-	-	-	-	-	-	-	-	35.72	-	100
UCR	FeO	Ulv-5	-	-	-	-	-	-	-	-	71.3	-	-	-	27.73	-	-	-	-	-	99.03
UCR	FeO	Ulv-5	-	-	-	-	-	-	-	1.95	69.23	-	-	-	27.54	-	0.39	-	-	-	99.11
UCR	Bn	Ulv-5	-	-	-	-	-	-	-	63.26	10.05	-	-	-	-	-	24.3	-	-	-	97.6
UCR	Bn	Ulv-5	-	-	-	-	-	-	-	60.72	12.6	-	-	-	-	-	24.79	-	-	-	98.11
UCR	Cct	Ulv-5	-	-	-	-	-	-	-	75.76	1.87	-	-	-	-	-	20.07	-	-	-	97.7
UCR	Cct	Ulv-5	-	-	-	-	-	-	-	77.96	1.02	-	-	-	-	-	20.65	-	-	-	99.63
UCR	Brt	Ulv-14	-	-	-	-	-	-	-	-	-	-	-	-	26.12	-	14.39	-	-	-	98.97
UCR	Cct	Ulv-14	-	-	-	-	-	-	-	77.54	0.36	-	-	-	-	-	21.51	-	-	-	99.42
UCR	Cv	Ulv-14	-	-	-	-	-	-	-	80.62	-	-	-	-	-	-	20.8	-	-	-	101.42
UCR	FeO	Ulv-14	-	-	-	-	-	-	-	-	0.71	-	-	-	-	-	-	-	-	-	100
UCR	FeO	Ulv-14	-	-	-	-	-	Ti: 2.64	-	-	67.8	-	-	-	29.56	-	-	-	-	-	100
UCR	FeO	Ulv-14	-	-	-	-	-	-	-	-	73.61	-	-	-	-	-	-	-	-	-	100

Atoms per formula unit	Ag	As	Au	Ba	Bi	Cl	Co	Cu	Fe	Hg	Mo	Ni	O	Pb	S	Se	Te	Zn	Total
	-	-	0.001	-	-	-	-	-	1.322	-	-	-	-	-	2.675	-	-	0.002	4
	0.001	-	-	-	-	-	-	0.965	0.982	-	0.055	-	-	-	1.994	0.001	-	0.002	4
	0.178	-	-	-	-	-	-	4.788	0.992	-	-	-	-	-	4.035	-	-	0.006	10
	0.023	-	0.001	-	-	-	-	4.988	0.995	-	-	-	-	-	3.990	-	-	-	10
	-	-	-	-	-	-	-	4.702	1.261	0.001	-	-	-	-	4.023	0.004	0.003	0.006	10
	0.007	-	-	-	-	-	-	4.940	0.984	0.002	0.101	0.002	-	-	3.953	0.008	0.001	0.003	10
	-	-	-	-	-	-	-	4.970	0.965	-	0.114	0.003	-	-	3.912	0.027	-	0.008	10
	0.005	-	-	-	-	-	0.001	1.845	0.023	-	0.000	-	-	-	1.123	0.000	-	0.001	3
	0.003	-	-	-	-	-	-	1.945	0.005	-	0.026	-	-	-	1.013	0.003	-	0.003	3
	0.000	-	-	-	-	-	-	1.944	0.001	0.001	0.025	-	-	-	1.018	0.006	-	0.004	3
	0.012	-	-	-	-	-	-	9.166	0.016	-	-	-	-	-	4.794	-	-	0.012	14
	0.041	-	-	-	-	-	-	8.648	0.096	-	-	-	-	-	5.207	-	-	0.008	14
	0.003	-	-	-	-	-	-	0.982	0.205	-	-	-	-	-	0.808	-	-	0.001	2
	0.001	-	-	-	-	-	-	0.990	0.205	-	-	-	-	-	0.801	-	-	0.002	2
	-	-	0.001	-	-	-	-	-	1.013	-	-	-	-	-	1.985	-	-	-	3
	0.005	-	-	-	-	-	0.005	0.094	1.220	-	0.043	0.010	-	-	1.619	0.002	-	0.001	3
	-	-	-	-	-	-	-	0.002	0.011	-	-	-	-	0.997	0.990	-	-	-	2
	0.002	-	-	-	0.000	-	-	0.065	0.018	-	-	-	-	0.970	0.885	0.058	-	-	2

0.100	-	-	0.000	-	-	0.054	0.020	-	0.002	-	-	0.898	0.046	0.879	-	-	2
0.010	-	-	0.000	-	-	0.075	0.011	-	0.003	-	-	0.949	0.134	0.817	-	-	2
-	-	-	0.000	-	-	-	0.000	-	1.297	-	-	-	2.703	-	-	-	4
-	1.043	-	-	-	0.018	0.039	0.047	-	-	0.908	-	-	0.945	-	-	-	3
0.001	0.876	-	0.001	-	0.849	-	0.143	-	-	0.020	-	-	1.102	0.008	-	-	3
0.001	0.887	-	0.000	-	0.848	-	0.127	-	0.024	0.019	-	-	1.087	0.007	-	-	3
-	-	-	0.807	-	-	0.152	0.020	-	-	0.001	-	-	0.019	0.001	-	-	1
-	-	-	-	Cd=0.006	-	0.011	0.132	-	-	-	-	-	1.002	-	-	0.849	2
-	-	-	-	Cd=0.010	-	0.009	0.118	-	-	-	-	-	0.994	-	-	0.869	2
-	-	-	-	-	-	0.007	0.121	-	-	-	-	-	1.024	-	-	0.917	2
-	-	-	-	-	-	0.015	0.136	-	-	-	-	-	1.063	-	-	0.877	2
-	-	-	-	Cd=0.007	-	0.011	0.132	-	-	-	-	-	0.990	-	-	0.860	2
-	-	-	-	-	0.003	0.011	0.122	-	-	0.001	-	-	0.973	-	-	0.889	2
0.933	-	-	-	-	-	-	-	0.067	-	-	-	-	-	-	-	-	1
0.923	-	-	-	-	-	-	-	0.077	-	-	-	-	-	-	-	-	1
0.992	-	-	-	-	-	0.005	-	-	-	-	-	-	0.001	-	-	-	1
2.024	-	-	-	-	-	0.012	-	-	-	-	-	-	0.964	-	-	-	3
1.998	-	-	-	-	-	-	-	-	-	-	-	-	1.002	-	-	-	3
1.056	-	-	-	-	-	0.954	0.015	-	-	-	-	-	0.975	-	-	-	3
0.964	-	-	-	-	-	1.065	-	-	-	-	-	-	0.971	-	-	-	3

1.429	-	-	-	-	0.511	-	0.009	-	-	-	-	-	-	0.051	-	-	-	2
1.960	-	-	-	-	-	-	0.096	-	-	-	-	-	-	-	-	0.944	-	3
2.014	-	-	-	-	-	-	0.167	-	-	-	-	-	-	-	-	0.819	-	3
1.841	-	-	-	-	-	-	0.104	-	-	-	-	-	-	-	-	1.054	-	3
1.861	-	-	-	-	-	-	0.188	-	-	-	-	-	-	-	-	0.951	-	3
1.896	-	-	-	-	-	-	0.167	-	-	-	-	-	-	-	-	0.937	-	3
-	-	-	-	-	-	-	-	0.848	-	-	-	1.152	-	-	-	-	-	2
-	-	-	-	-	-	-	0.020	0.825	-	-	-	1.146	-	0.008	-	-	-	2
-	-	-	-	-	-	-	5.149	0.931	-	-	-	-	-	3.920	-	-	-	10
-	-	-	-	-	-	-	4.889	1.154	-	-	-	-	-	3.957	-	-	-	10
-	-	-	-	-	-	-	1.931	0.054	-	-	-	-	-	1.014	-	-	-	3
-	-	-	-	-	-	-	1.948	0.029	-	-	-	-	-	1.023	-	-	-	3
-	-	-	1.019	-	-	-	-	-	-	-	-	3.907	-	1.074	-	-	-	6
-	-	-	-	-	-	-	1.929	0.010	-	-	-	-	-	1.061	-	-	-	3
-	-	-	-	-	-	-	1.323	-	-	-	-	-	-	0.677	-	-	-	2
-	-	-	-	-	-	-	-	2.000	-	-	-	-	-	-	-	-	-	2
-	-	-	-	-	0.047	-	-	0.774	-	-	-	1.178	-	-	-	-	-	2
-	-	-	-	-	-	-	-	2.000	-	-	-	-	-	-	-	-	-	2

*Note: Am – amalgam, Arg – argentite, Bn – bornite, Brt – barite, Cbt – cobaltite, Ccp – chalcopyrite, Cct – chalcocite, Clag – chlorargerite (*Cl is not precisely measured), Cst – clausthalite, Cv – covellite, Dg – digenite, FeO - iron oxide, Ga – galena, Gf – gersdorfite, Hs – hessite, Mol - molybdenite, Py - pyrite, Sph - sphalerite, Stm – stromeyerite.*

Laboratories: IGG – Institute on Geology and Geophysics, Republic of Uzbekistan; UCR – University of California, Riverside; UiO – University of Oslo; UiT - The Arctic University of Norway

Fluid-inclusion study

In total, about 80 fluid inclusions (FIs) hosted by vein (Figs. 7 & 8; Electronic Supplement 2, 3) and host-rock quartz from the Nussir and Ulveryggen deposits, respectively, were analysed. For the fluid inclusions in quartz from the Ulveryggen deposit, only a limited amount of data was collected due to the scarcity of sufficiently large transparent crystals associated with the mineralisation. Consequently, most of the fluid-inclusion data were collected from the mineralised intervals within metatuffite (Fig. 8A) and metasiltstone (Fig. 8B) in the Nussir deposit. Multiple generations of fluid inclusions have been recognised in quartz veins hosted by both lithologies. The studied inclusions have been described as primary or secondary in their origin, applying the diagnostic criteria proposed by Roedder (1984). Primary inclusions show very diverse phase relations at room temperature. Based on phases present at room temperature, fluid inclusions have been classified into the following types: Type 1 - liquid-rich two-phase (L + V) inclusions, Type 2 - polyphase (L + V + S) inclusions, Type 3 - two-phase (L + S) inclusions, Type 4 - liquid-only (L) inclusions, and Type 5 - vapour-only (V) inclusions (Fig. 7E–H), where L, V, and S stand for liquid, vapour and solid phase, respectively.

The majority of fluid inclusions have sizes less than 10 µm across and show irregular to subrounded shape. At room temperature, vapour bubbles occupy about 25% of the volume in fluid inclusions of Types 1 and 2. The solid phase (daughter crystal) is transparent, isotropic, and usually occupies about 20 to 25% of the volume in Type 2 fluid inclusions. In Type 3 fluid inclusions, the daughter crystal occupies up to 30% of the volume.

Type 1 inclusions are present in quartz from both the Nussir and the Ulveryggen deposits. In the Nussir deposit, they have a wide range of homogenisation temperatures (168–430°C) and a low salinity (0.4–3.2 wt.% NaCl equiv.). The Ulveryggen deposit Type 1 FIs show an even wider range of homogenisation temperatures (102–550°C) and a higher salinity (13.9 wt.% NaCl equiv.). Type 2 FIs prevail over all other types of fluid inclusions. These are further subdivided into three subtypes according to their homogenisation mode: FIs of Type 2a homogenise into liquid with vapour disappearing as the last phase, FIs of Type 2b homogenise by salt dissolution, and FIs of Type 2c have both vapour and salt disappearing at the same temperature. FIs of Type 2a homogenise at 247–350°C and their salinity varies from 30 to 36

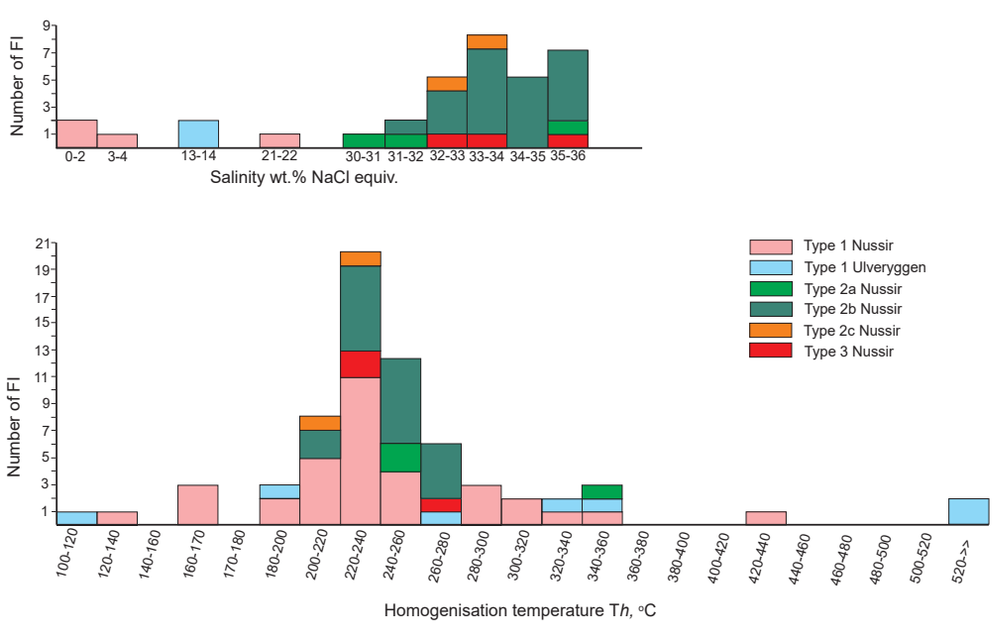

Figure 7. Histograms illustrating ranges of variation in homogenisation temperature and salinity obtained from FIs. Note that different colours are assigned to different types of FIs (see the text for further details) for the Nussir and Ulveryggen deposits.

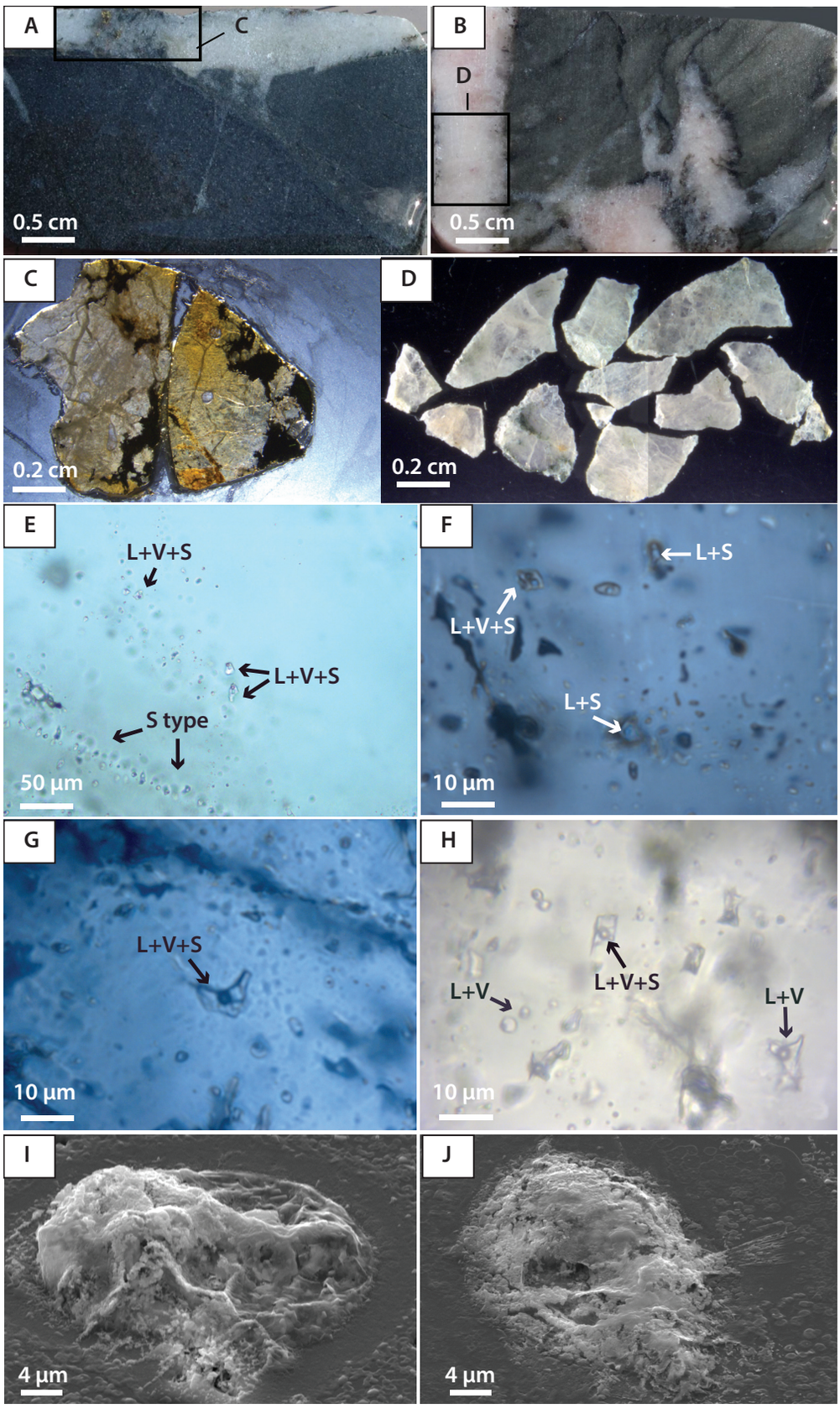

Figure 8. (A) Photograph of the sample NS-45, metatuffite from HCVR crosscut by quartz-carbonate vein; (B) photograph of the sample NS-39 metasiltstone cross-cut by quartz vein; (C) photograph of the quartz double-side polished wafer (NS-52) from the sample NS-45; (D) photograph of the double-side polished wafter (NS-51A-J) from the sample NS-39; (E–H) photomicrographs illustrating FIs in quartz. S-type – secondary inclusions, L + V + S – liquid + vapour + salt; L + S – liquid + salt; L + V – liquid + vapour; (I & J) backscattered electron image of decrepitated evaporate mounds formed by overheating of FIs.

wt.% NaCl equiv. FIs of Type 2b homogenise at temperatures between 200 and 270°C and have salinities ranging from 31 to 36 wt.% NaCl equiv. FIs of Type 2c have salinity ranging between 32 and 34 wt.% NaCl equiv. and homogenise at 200–240°C.

Type 3 FIs are found in the quartz of the Nussir deposit. The final halite melting temperature ranges from 220 to 260°C indicating a salinity between 32 and 35 wt.% NaCl equiv. Types 4 and 5 FIs occur as isolated FI clusters and do not indicate a boiling phenomenon.

Secondary inclusions are of types 1 (L + V) and 2a (L + V + S, and homogenise into liquid with vapour as the last phase, Fig. 8E). They are found along cracks in the vein quartz. Secondary FIs have rounded and subrounded shapes and are about 1–3 μm in size. Vapour bubbles occupy about 25% of volume of the type 1 fluid inclusions at room temperature. For the type 2 secondary FIs, the vapour bubble occupies around 10% of the inclusion and the solid phase occupies around 10–15% of the inclusion. The homogenisation temperature of the type 1 secondary FIs varies from 150 to 220°C. The type 2a secondary FIs homogenise at 200–220°C. The salinity of these FIs is hard to measure due to their small size.

Decrepitated fluid-inclusion analysis showed that the evaporate mounds formed from primary fluid inclusions have complex chemical composition including Na, Ba, Mg, Mn, Ca, K and Cl (Figs. 8I, J, 9 & 10, Table 5). In addition, minor amounts of Ni, Fe, S and Cu were detected, suggesting that these fluids were metal-bearing. Evaporate mounds that formed after decrepitation of secondary inclusions contain Ca, Ba, Mn, Ti, Fe, S and Cl (Fig. 10).

Table 5. Chemical data for selected decrepitated evaporate mounds obtained with EDS detector (wt%).

Sample	Al	Ba	Br	Ca	Cl	Cu	Fe	K	Mn	Na	O	S	Si	Total
NS-51-d-36	0.41	7.3	-	5.96	0.17	-	4.86	-	3.98	0.56	44.8	2.89	29.95	100.9
NS-51-d-37	0.27	0.95	-	9.43	0.27	0.25	6.22	0.17	4.56	1.49	45.06	1.41	30.82	100.89
NS-51-d-38	-	4.98	-	7.95	0.45	-	1.37	-	1.59	0.43	46.83	2.04	34.25	99.89
NS-51-d-39	-	0.35	-	7.61	0.45	-	2.75	-	1.69	0.46	48.77	1.1	37.4	100.57
NS-51-d-40	0.29	0.39	-	10.96	0.53	-	1.27	-	1.37	0.63	48.06	1.87	34.76	100.14
NS-51-d-41	0.28	0.65	-	7.94	0.29	-	4.92	0.13	3.63	0.82	47.01	0.94	34.52	101.14
NS-51-d-42	-	9.48	-	5.55	0.18	-	2.08	-	1.74	0.64	46.66	3.14	32.76	102.23
NS-51-d-43	-	0.7	0.36	9.42	0.49	0.22	4.34	0.13	2.37	1.15	46.19	1.69	32.83	99.9
NS-51-d-44	0.34	8.28	-	5.36	0.23	-	5.02	0.11	3.14	0.61	42.9	2.96	28.51	97.45

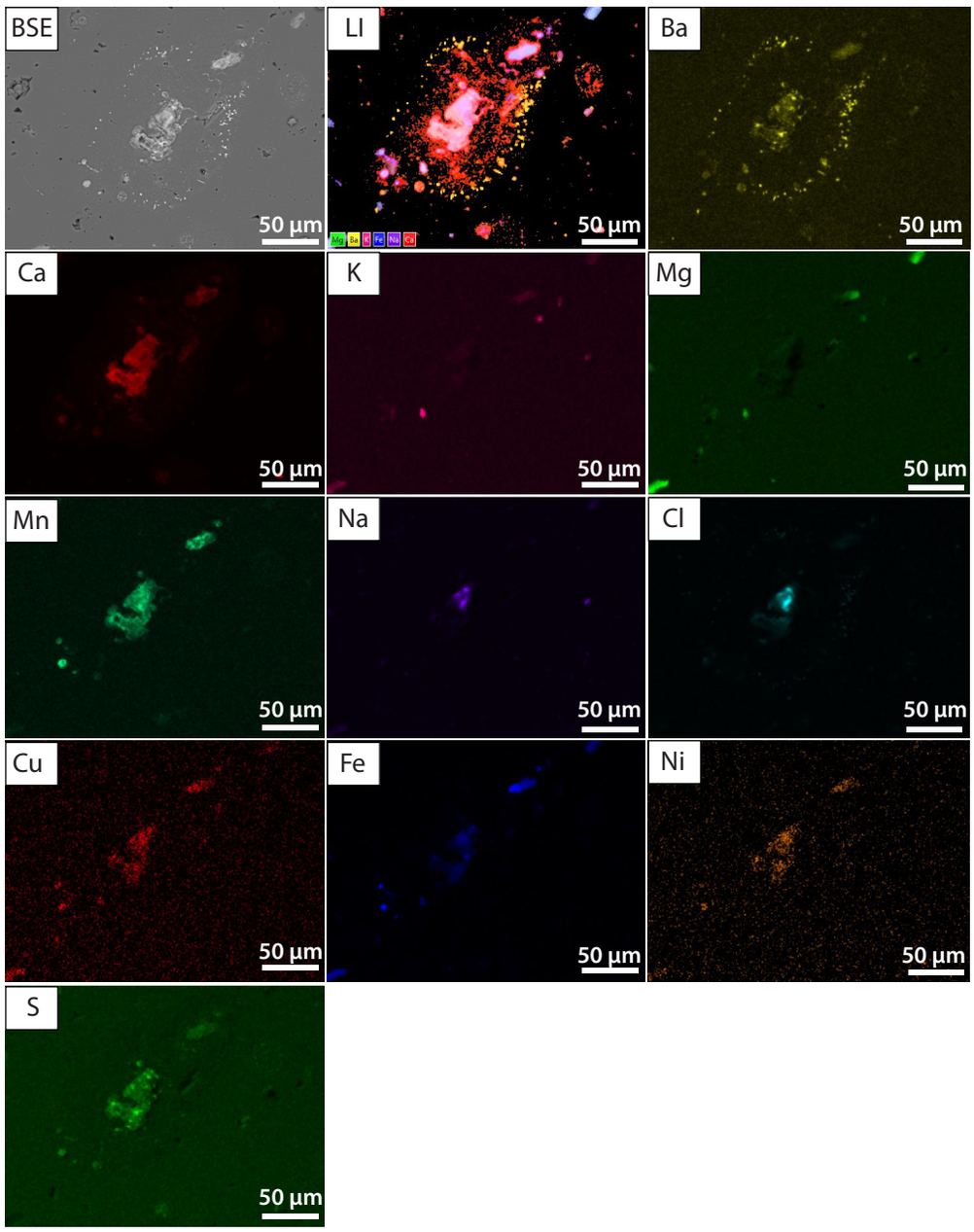

Figure 9. Element mapping of a decrepitated fluid inclusion in vein quartz from the Nussir deposit (sample NS-51). BSE – backscatter electron image, LI – overlay of elemental maps.

Stable isotopes

Carbon and oxygen isotope values were measured for 12 samples of the dolomitic marble hosting the mineralisation, as well as from the ore-bearing veins of the Nussir deposit (Fig. 11, Table 6). $\delta^{13}C$ values for the host dolomitic marble range from + 1.8 to + 2.9‰ V-PDB, and $\delta^{18}O$ values range from - 18.2 to - 15.9‰ V-PDB. Ore-bearing vein dolomite from the Nussir deposit has $\delta^{13}C$ values ranging from - 1.0 to + 2.3‰ and $\delta^{18}O$ values varying from - 17.0 to - 16.0‰. Two samples from a nonmineralised metalimestone from the Vargsund Formation in the Porsa Group were also analysed, and the results are provided here for comparison. Metalimestone has slightly higher $\delta^{13}C$ and $\delta^{18}O$ values, ranging from + 3.1 to + 3.2‰ and from - 9.6 to - 9.5‰, respectively.

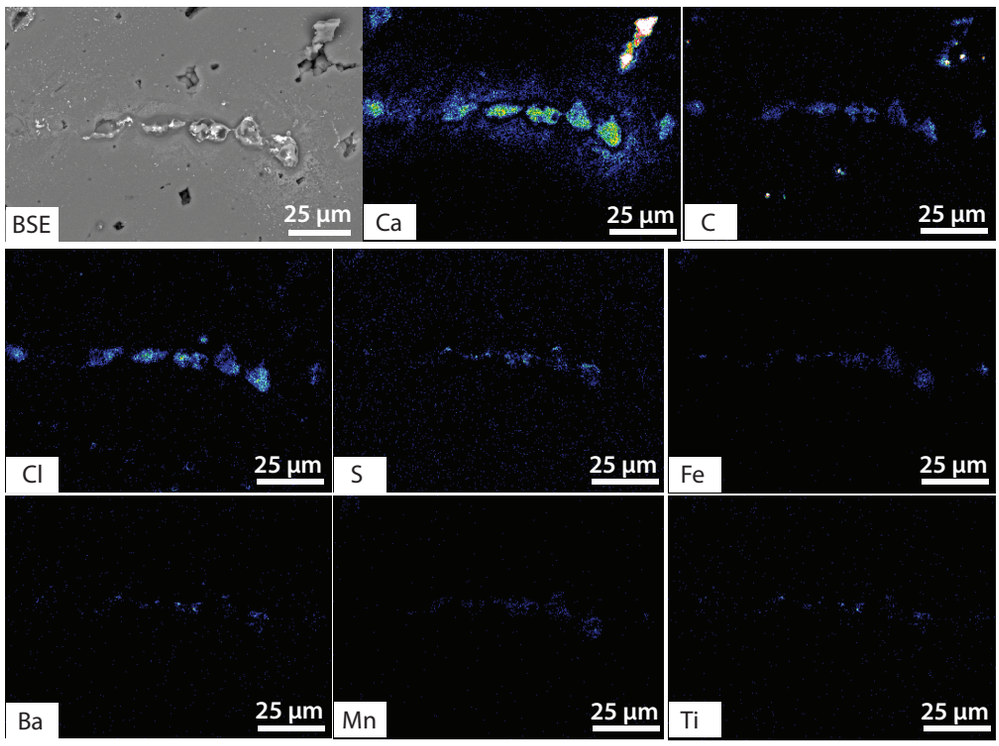

Figure 10. Images illustrating elemental distribution in decrepitated secondary fluid inclusion in vein quartz from the Nussir deposit. Brightness illustrates the intensity of the signal (sample NS-51). BSE – backscatter electron image.

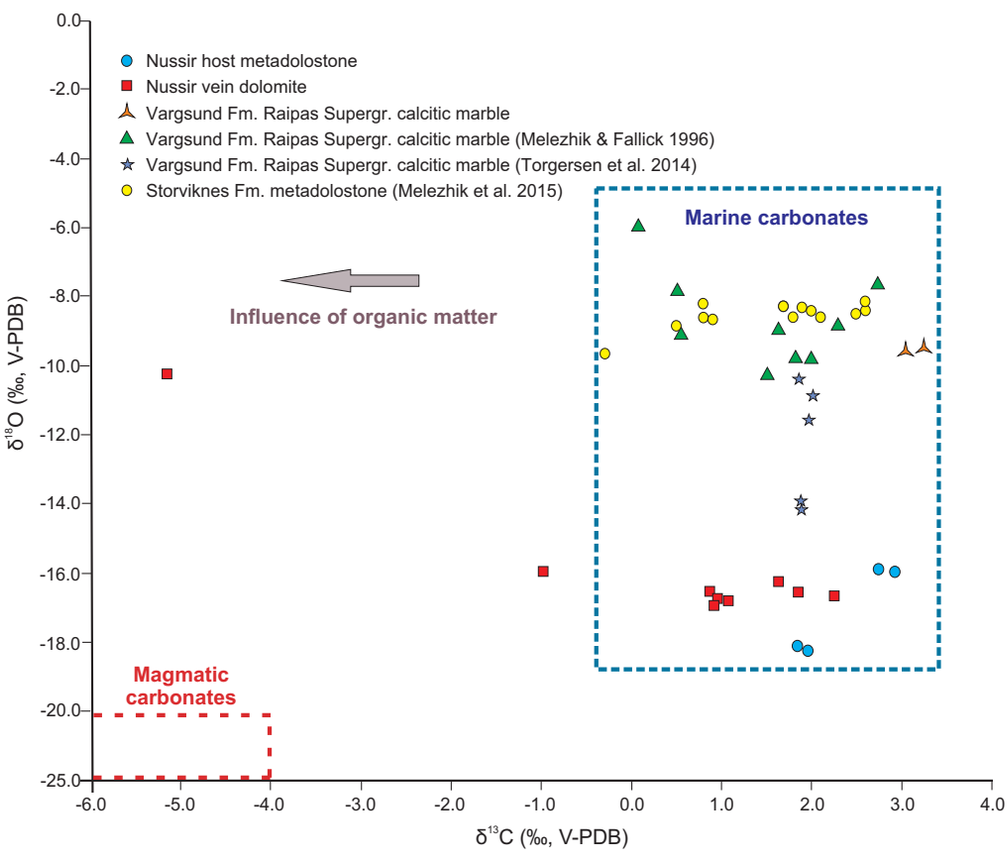

Figure 11. Scatter diagram of $\delta^{13}C$ (V-PDB) vs. $\delta^{18}O$ (V-PDB) values illustrating the source of carbon and oxygen for the studied carbonate samples and the data obtained in the previous studies in the RTW (Torgersen et al. (2014); Melezhik & Fallick (1996); Melezhik et al. (2015)) and those for magmatic carbonates (Stakes & O'Neil, 1982).

Table 6. Carbon and oxygen isotope composition of host dolomitic marble and ore-bearing carbonate veins. V-PDB – Vienna Pee Dee Belemnite.

Sample #	Sample description	"$\delta^{13}C$ (‰, VPDB) "	"$\delta^{18}O$ (‰, VPDB)"
Gorahatjohka Formation, Saltvatn Group, Nussir Deposit, Repparfjord			
*NS-31A	host dolomite	2.7	-15.9
*NS-31B	host dolomite	2.9	-16.0
*NS-16	host dolomite	2.0	-18.3
*NS-17	host dolomite	1.8	-18.2
*NS-24 4	vein dolomite	1.6	-16.3
*NS-24 3	vein dolomite	1.9	-16.6
*NS-24 2	vein dolomite	2.3	-16.7
*NS-24 1	vein dolomite	-1.0	-16.0
*NS-32 4	vein dolomite	0.9	-17.0
*NS-32 3	vein dolomite	1.1	-16.8
*NS-32 2	vein dolomite	0.9	-16.6
*NS-32 1	vein dolomite	1.0	-16.8
Vargsung Formation, Raipas Group, Repparfjord			
*PO-14-1	calcite	3.1	-9.6
*PO-14-2	calcite	3.2	-9.5
Vargsund Formation, Raipas Group, Repparfjord (Melezhik & Fallick, 1996)			
RF-2	dolostone	1.5	-10.2
RF-3	dolostone	1.8	-9.8
RF-7	dolostone	2.0	-9.8
RF-8	dolostone	2.7	-7.6
RF-9	dolostone	-5.2	-10.3
RF-13	dolostone	0.6	-9.1
RF-14	dolostone	1.6	-9.0
RF-16	dolostone	0.1	-6.0
RF-17	dolostone	0.5	-7.9
RF-18	dolostone	2.3	-8.8
Vargsund Formation, Raipas Group, Kvenklubben Fault, Repparfjord (Torgersen et al. 2014)			
ETO 113	dolostone	1.9	-14.0
ETO 114	dolostone	1.9	-14.1
ETO 115	dolostone	2.0	-11.6
ETO 116	dolostone	2.0	-10.9
ETO 119	dolostone	1.9	-10.4

Storviknes Formation, Raipas Group, Alta-Kvænangen Window (Melezhik et al., 2015)			
RP_14	dolostone	-0.3	-9.7
RP_1	dolostone	1.9	-8.3
RP_2	dolostone	2.1	-8.6
RP_3	dolostone	2.0	-8.4
RP_4	dolostone	1.8	-8.6
RP_5	dolostone	1.7	-8.3
RP_6	dolostone	2.6	-8.4
RP_7	dolostone	2.3	-8.9
RP_8	dolostone	2.6	-8.2
RP_9	dolostone	2.5	-8.5
RP_10	dolostone	0.8	-8.6
RP_11	dolostone	0.9	-8.7
RP_12	dolostone	0.5	-8.9
RP_13	dolostone	0.8	-8.2

** UCR*

** UiT*

Note: VPDB – Vienna Pee Dee Belemnite

Discussion

Sulphide mineralisation at the Nussir and Ulveryggen deposits

Despite the numerous geological studies in the Nussir and Ulveryggen areas, remarkably little is known about the ore-forming processes that led to the Cu mineralisation (e.g., Sandstad et al., 2007; Sandstad, 2010; Perelló et al., 2015; Torgersen et al., 2015a). Although the Nussir and Ulveryggen deposits are considered to be the products of the same mineralising event, they show significant differences in the style of the mineralisation, predominantly controlled by differences in the host-rock lithology of these two deposits. The less permeable volcano-sedimentary succession in the Nussir area focused the fluid flow and deposited the mineralisation mostly in the form of quartz-carbonate veins (Figs. 5C & 8A). In contrast, the porous arkosic metasandstones at the Ulveryggen deposit did not have a capacity to focus fluid flow. The circulating fluids thus penetrated through the whole succession, resulting in disseminated mineralisation in the form of cement along grain boundaries and around only few veins (Fabricius, 1979; Sandstad et al., 2007).

Studied drillcores from the Nussir volcano-sedimentary sequence suggest a vertical zoning in distribution of Cu-bearing sulphides. In the upper part of the sequence, chalcopyrite dominates, and at the top of the NS-DD-08-006 drillcore, galena and silver minerals are also found. Deeper in the sequence, pyrite was gradually replaced by chalcopyrite (Fig. 6H), bornite, digenite, chalcocite and covellite. The Ulveryggen deposit is different to some extent as no sulphide zoning was observed in our study. However, vein-

type mineralisation hosted by a series of shear zones was described by Sandstad et al. (2007) from the Ulveryggen deposit. In these shear zones, Cu-sulphide mineralisation is associated with quartz veins and has a zonal distribution across stratigraphy and also laterally. Therefore, shear zones might have acted as fluid pathways and controlled zonal sulphide distribution (cf., Perelló et al., 2015). In addition, while Stribrny (1985) documented chalcopyrite as the dominant copper sulphide, our study found that bornite is also abundant. Therefore, lateral zoning of copper sulphides might also be developed in the Ulveryggen deposit, but further detailed investigation is needed to explore this interpretation.

Source for base metals: metamorphosed redbeds or hosting volcanic rocks?

Both deposits have undergone greenschist to lower amphibolite-facies metamorphism and significant deformation (Torgersen et al., 2015a; this study). Petrographic study of the host rocks from the Nussir deposit reveals abundant chlorite and sericite. Chlorite mostly replaced biotite reflecting its formation during the retrograde metamorhic stage. Deformation structures including crenulation cleavage in mica-rich beds and sigmoidally shaped aggregates of quartz and carbonate as well as elongated grains of quartz in veins and recrystallised quartz, suggest that the succession was affected by compression after its deposition (Fig. 5E, D). At least two generations of mineralised quartz-carbonate veins indicate two or more discrete hydrothermal events (Fig. 5D–F, Sandstad, 2010).

In the Ulveryggen deposit, the host lithology is changing laterally across the deposit from coarse grained, as described by Stribrny (1985), to fine grained as observed in this study. Greenschist-facies metamorphism resulted in the formation of mica-rich layers, sericitisation of feldspar fragments (Fig. 5G, H) and chloritisation. Both brittle and ductile deformation styles and mineralised major shear zones were observed by Sandstad et al. (2007).

A. Alteration of mafic volcanic rocks as a potential source of metals?

Alkaline mafic intrusions have been recognised as a potential source of chalcophile metals in several sediment-hosted copper deposits worldwide (Brown, 1984, 1992; Carmichael & Ghiorso, 1986; Keith et al., 1997; Hitzman et al., 2005, 2010). For example, at the Kipushi Zn–Cu deposit in DRC (Heijlen et al., 2008), which shares many similarities with the Nussir and Ulveryggen deposits, mafic volcanics were inferred as one of the possible sources for metals that were leached out by highly saline brines during their deep convection and subsequent drainage along the Kipushi Fault.

Jensen (1996) and Pharaoh & Brewer (1990) described mafic intrusions in the RTW with alkaline compositions. The whole-rock geochemical data (Tables 1–3) were used to construct the isocon diagrams according to the method developed by Grant (1986, 2005). The constructed isocon diagrams compare concentrations for a suite of mobile and immobile elements in nonmineralised vs. mineralised samples and illustrate their geochemical behaviour in response to the mineralisation processes at the Nussir and Ulveryggen deposits. Volcanic and carbonate-siliciclastic rocks were plotted on different graphs (Fig. 12A–C). The Nussir samples NS-13 and NS-15 were chosen as nonmineralised samples for mafic volcanic and carbonate-siliciclastic rocks, respectively, since they contain the lowest amounts of Cu. The Ulveryggen sedimentary rocks contain disseminated mineralisation with the lowest concentration of Cu in the YM-03 sample (2610 ppm). Therefore, the YM-03 sample was chosen as a nonmineralised sample for the Ulveryggen deposit. The whole-rock geochemistry demonstrates that the Cu

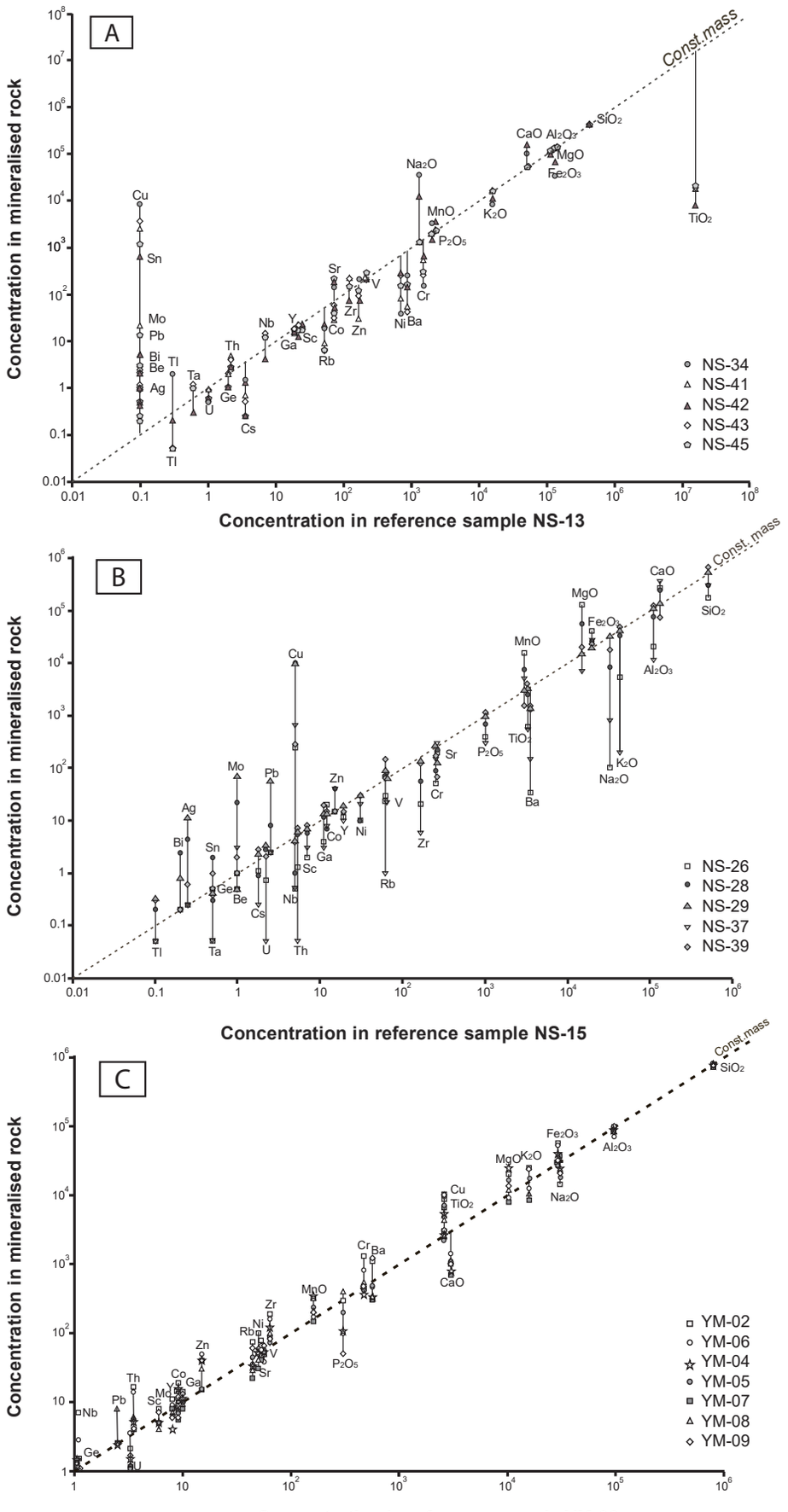

Figure 12. Isocon diagrams illustrating the elemental mass change in mineralised rocks with respect to non-mineralised rock (see the text for explanation) in (A) volcanic rocks from the Nussir deposit; (B) carbonate-siliciclastic rocks from the Nussir deposit; (C) host rocks from the Ulveryggen deposit; YM-03 is taken as a reference sample since it has the lowest concentration of Cu.

mineralisation at the Nussir deposit is associated with higher CaO contents, i.e., with carbonisation, whereas at the Ulveryggen deposit Ca was likely leached out with hydrothermal fluids (due to the reaction of ore-bearing fluids with carbonate rocks, Table 3). This is in agreement with Sandstad (2010) who suggested that the Cu mineralisation in the Ulveryggen deposit is hosted in carbonate-rich rocks. In addition, a petrographic study revealed that carbonate-rich volcanic rocks that are observed at shallow depth in the NS-08/06 drillcore (Fig. 3) are also enriched in Cu. In the Nussir deposit, Na_2O is generally higher in mineralised volcanics in comparison to nonmineralised rocks. This is an indication of either the reaction with saline fluids enriched in NaCl or albitisation. K_2O concentration tends to be slightly higher in nonmineralised volcanic rocks at the Nussir deposit. In contrast, the rocks of the Ulveryggen deposit do not show any significant changes in Na_2O and K_2O contents. The redistribution of Na_2O and K_2O and homogenisation of their contents might have occurred later during the regional greenschist-facies metamorphism.

B. Metamorphosed redbeds as a potential base-metal source for the Nussir and Ulveryggen deposits

Redbed sandstones (hematite-coated quartz- and feldspar-rich sediments) are commonly considered as a critical component for the formation of sediment-hosted Cu deposits as a source of base metals including copper (e.g., Kirkham, 1989; Hitzman et al., 2005, 2010) and for maintaining oxidising conditions in the basin necessary for the metal transport. The redbed-associated deposits include Kupferschiefer (Germany, Poland), Zambian Copper Belt (Zambia), Zairian Copperbelt (DRC), Redstone Copperbelt (Canada), Kodaro–Udokan Belt (Siberia, Russia), Kalahari Copperbelt (Namibia and Botswana), White Pine (Michigan, USA), Donchuan (China) and a number of smaller deposits (Brown, 1971; Ripley et al., 1980; Chartrand & Brown, 1985; Selley et al., 2005; Dewaele et al., 2006; Brems et al., 2009; El Desouky et al., 2009; Sillitoe et al., 2010). Iron for the diagenetically formed hematite is inferred to be derived from dissolution of unstable ferromagnesium minerals and infiltration of oxidised meteoric waters (Bankole et al., 2016).

The major difference between the Nussir and Ulveryggen deposits and similar sediment-hosted Cu deposits worldwide is an absence of associated redbeds in the former. Gablina (1990) and Eriksson & Cheney (1992) suggested that Precambrian sedimentary sequences lost their original reddish coloration due to metamorphic transformation of hematite to magnetite. Even though redbeds have not previously been described in the RTW, some features such as abundant magnetite, red to violet colour of meta-conglomerate (Stribrny, 1985), and prevalence of iron oxides over pyrite at the Ulveryggen deposit suggest that the metaconglomerates and metasandstones of the Ulveryggen deposit might be meta-morphosed redbeds. Stribrny (1985) described red to violet beds and disseminated hematite in the variegated metaconglomerate. Furthermore, hematite and magnetite are the most abundant minerals after chalcopyrite among the opaque minerals (Stribrny, 1985). Pyrite is also abundant at the Ulveryggen deposit. However, the predominance of iron oxides over pyrite suggests that the depositional redox conditions were oxidising. Furthermore, magnetite forms rims around detrital chromite grains. SEM analysis of the Ulveryggen deposit metasandstone performed in this study indeed indicated the presence of a significant amount of magnetite; however, the grains looked to be detrital rather than authigenic in origin. In addition, the whole-rock geochemical analyses (Table 3) record a relatively high total iron content in arkosic metasandstone (up to 5.65 wt.%), which is consistent with their origin as metamorphosed redbeds. Matthews (1976) calculated minimum P–T conditions of 365°C and 1.5 kbars for the full conversion of hematite into magnetite. Assuming that the inferred P–T conditions for the Nussir deposit (330–340°C and 1.1–2.7 kbars; see discussion below) are also applicable to the Ulveryggen deposit, temperatures did not reach 365°C (at 1.5 kbars) to transform all hematite to magnetite in the metaconglomerate of the Ulveryggen deposit.

P–T–X conditions

The fluid-inclusion (FI) study was conducted with the main goal to get a better insight into the nature of the transport media for Cu and associated metals. Fig. 13 shows temperature vs. pressure isochores, calculated from homogenisation temperature (Th) and salinity of the FIs. To simplify, only end-member isochores for each type of FIs are plotted on Fig. 13. Multiple generations of FIs and very diverse FI assemblages reflect a complex and potentially multistage evolution of the hydrothermal fluids that circulated through the rocks of the Nussir and Ulveryggen areas. Here, we discuss FI data for the Nussir deposit and refer to the data of Fabricius (1979) for FIs from the Ulveryggen deposit. The two-phase (L + V, Type 1) fluid inclusions from the Nussir deposit show a very broad range of homogenisation temperatures, but a relatively narrow range of salinities (Fig. 8). The low salinity of the entrapped fluids (<3.2 wt.% NaCl equiv.) limited their capacity to transport metals such as Cu and Zn, since these elements are typically transported in the form of Cl-complexes (Seward et al., 2013). In contrast, FIs that belong to the Types 2 and 3 entrapped highly saline hydrothermal fluids, with a greater capacity to transport base metals. The SEM-EDS analyses of the Type 2 FIs confirmed that they contain detectable amounts of Cu, Fe and Ni (Fig. 9). The microthermometry data were used for construction of representative isochores for the fluid inclusions of Types 1, 2, and 3 (Fig. 13). To define the P–T conditions of the main mineralising event, the isochores of the Type 2 FIs should be intersected by an independent geothermometer. In this study, the sphalerite geothermometer described by Hutchison & Scott (1981) was applied (Equations 1 & 2):

(1 b) Log mole % of CuS in ZnS = 4.202 - 3735 T^{-1} (°K) (1)

(5 kb) Log mole % of CuS in ZnS = 4.084 - 3791 T^{-1} (°K) (2)

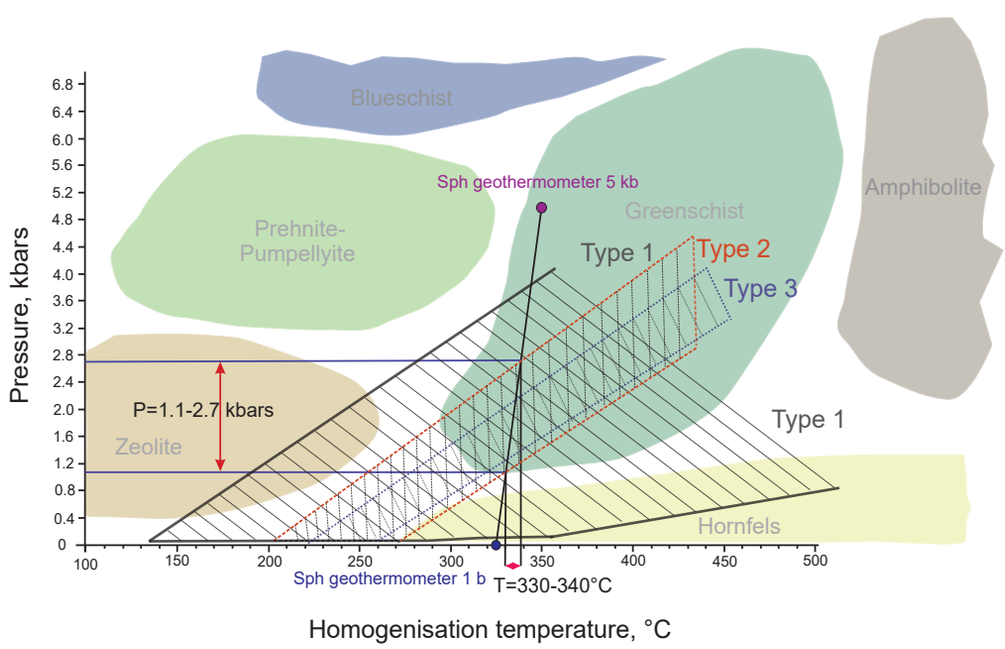

Figure 13. Pressure-temperature diagram illustrating conditions of formation of the Nussir mineralisation. Fields for the fluid inclusions are defined by the lower and upper isochores (lines corresponding to constant volume in the P–T field) derived from the data for the Type 1, Type 2 and Type 3 fluid inclusions. Average results of sphalerite geothermometry are represented by the line between 1 bar and 5 kbars. The inferred P–T conditions for formation of the deposit are defined by the intersection between this line of sphalerite geothermometry and the fields of the Type 2 and Type 3 fluid inclusions. Types 2 and 3 FIs represent ore-forming fluids. Generalised pressure-temperature domains for metamorphic facies are shown in the background.

The Cu content in sphalerite that was in chemical equilibrium with chalcopyrite ranges between 0.47 and 0.96 wt.%, suggesting mineralisation temperatures ranging between 320 and 350°C at 1 bar and between 335 and 370°C at 5 kbars. Hutchison & Scott (1981) observed that the solubility of CuS in sphalerite is almost unaffected by pressure. Considerable changes will be observed at temperatures exceeding 550°C at 1 b and 600°C at 5 kb. Combining isochores with the calculated mineralisation temperatures, the formation temperatures were constrained to a narrow range between 330 and 340°C, whereas the formation pressure spans the range between 1.1 and 2.7 kbars (Fig. 13). Assuming lithostatic pressure, the mineralisation occurred at a depth varying from approximately 3.4 to 9 km. The mineralisation either had a long and continuous history or evolved with multiple, episodic remobilisation events during progressive burial of the basin.

In our study, the main focus was on the fluid inclusions from the Nussir deposit. Fabricius (1979) studied petrography and microthermometry of fluid inclusions in quartz veins and quartz from the matrix of the Ulveryggen deposit. The L + V and L + V + S types of fluid inclusions were described. The wide range of reported homogenisation temperatures and salinities, ranging from 145 to 550°C and from 20 to 42 wt.% NaCl equiv., respectively, closely overlaps with the data obtained in this study (Figs. 8 & 13).

Na, Mg, K, Mn and Ca were the major cations in the fluids (Table 5, Figs. 9 & 10). The presence of Cu, Fe, Ni and Co suggests that these fluids were metal-bearing; in addition, S was found in the precipitated salts. The studied fluid inclusions represent at least one generation of metal-bearing fluids (primary FIs). In secondary fluid inclusions, Cu was not detected. However, both secondary and primary fluid inclusions are similarly enriched in Ba, Ca, Cl, Fe, K, Mg, Mn, Na and S. This suggests that the evolved fluids had a diminished Cu-bearing potential.

The source of fluids: evaporites in the sedimentary succession?

High-salinity fluids have been reported from other sediment-hosted Cu deposits (e.g., Hitzman et al., 2005; Cailteux et al., 2005; Heijlen et al., 2008). The source of salinity remains uncertain for many of these deposits and different interpretations have been proposed including evolved seawater, connate waters, gypsum dehydration and low-grade metamorphic dehydration as well as inflow of meteoric waters (e.g., Hitzman et al., 2005). The high salinities indicated by fluid inclusions from both the Nussir and the Ulveryggen deposits could reflect fluids derived from evaporite dissolution, contribution of magmatic fluids, or, alternatively, an effect of retrograde metamorphism involving rehydration of amphiboles and high-grade metamorphic minerals such as biotite (e.g., Bennett & Barker, 1992) in association with gradual cooling under constant pressure (Fig. 13).

Fig. 11 and Table 6 show $\delta^{13}C$ and $\delta^{18}O$ values for the host dolomitic marble and carbonates in the mineralised veins from the Nussir deposit. Based on carbon and oxygen isotope compositions, all carbonate samples analysed in this and previous studies from the RTW and Alta–Kvænangen Tectonic Window (AKTW) plot in the field of marine carbonates. Marbles from the Palaeoproterozoic Vargsund Formation show ^{13}C-enrichment, likely reflecting temporal variations in the C-isotope composition of seawater. While O isotope values of both the host dolomitic marble and ore-bearing carbonates are more negative than those of other Palaeoproterozoic unmineralised carbonates in the RTW, their C isotope values, with the exception of two outliers, are similar to each other and to those of other Palaeoproterozoic carbonates in the RTW and AKTW (Melezhik & Fallick, 1996; Torgersen et al., 2014; Melezhik et al., 2015).

Carbonate-fluid exchange primarily affects oxygen isotope values and only at a higher water-rock ratio C isotope values in carbonates (cf., Banner & Hanson, 1990). The data indicate a rock-buffered system with most of the carbon in veins derived from the host dolostones with little or no CO_2 contributed by magmatic, hydrothermal or organic sources.

Brine derivation from retrograde metamorphism of highly metamorphosed rocks is not supported by field and petrographic observations, as the highest degree of metamorphism reported in the area is amphibolite facies. We rather suggest that dissolution of evaporites led to formation of highly saline brines. Although evaporites have not been reported in the RTW, sulphate-bearing evaporites were described in the nearby and broadly correlative Alta–Kvænangen Tectonic Window (Melezhik et al., 2015; Nasuti et al., 2015) as well as from the broadly correlative sedimentary successions in Fennoscandia and worldwide, deposited during the c. 2.2–2.06 Ga Lomagundi carbon isotope excursion in seawater composition (e.g., Bekker et al., 2006; Schröder et al., 2008; Melezhik et al., 2015). Furthermore, a significant increase in the seawater sulphate reservoir during the Lomagundi carbon isotope excursion has been inferred (Bekker & Holland, 2012; Planavsky et al., 2012), which ended at about the same time as deposition of the Raipas Supergroup started. Based on these correlations and evidence for evaporite deposition on the Fennoscandian Shield and worldwide at roughly the same time, we suggest that evaporites were also deposited in the RTW and were entirely consumed via dissolution in the basin subsequent to their deposition. We suggest that warm basinal fluids have been circulating through carbonate rocks, reaching equilibrium with carbonates via dissolution-precipitation. Evaporites, originally present in the volcano-sedimentary succession, were dissolved and thus enriched the basinal fluids in sulphate and chlorine. Hot (330–340°C), saline brines circulating through the volcano-sedimentary sequence leached Cu and other metals from mafic volcanic rocks and alkaline mafic intrusions. In addition, these fluids could have leached metals from redbeds in the Ulveryggen deposit. Reaching to the shallow levels in the basin, metal-charged saline fluids were cooled, sulphate was reduced, and metals were bounded with hydrogen sulphide and precipitated, following the reactions (Equations 3 & 4):

$$CaSO_4 + 2\ CH_2O\ (\text{organic matter}) \rightarrow CaCO_3 + CO_2 + H_2S + H_2O \quad (3)$$

$$CuCl_2 + H_2S \rightarrow CuS + 2\ H^+ + 2\ Cl^- \quad (4)$$

Copper sulphides could also be precipitated when Cu-rich fluids circulate through iron sulphide-rich beds as was described at White Pine in Michigan. This process commonly results in a Cu-sulphide rim around the pyrite, when the latter acts as a sink for Cu (Fig. 6H; Equation 5; Brown, 1971, 1992).

$$FeS_2 + CuCl_2 \leftrightarrow CuFeS_2 + 2\ Cl^- \quad (5)$$

Oxidising fluids transport sulphur in sulphate form (Hitzman et al., 2010). Although at the Nussir deposit the Cu mineralisation occurs in different lithologies, including dolomitic marbles, metasandstones, metasiltstones and, to some extent, volcanic rocks, the highest-grade mineralisation is hosted by dolomitic marbles and carbonatised intervals. Consequently, dolostones must have formed an efficient reducing front due to the presence of organic matter to promote reduction of sulphate to sulphide, resulting in precipitation of Cu-sulphide mineralisation. Similar processes have been described for numerous carbonate-hosted base-metal mineral deposits (e.g., Anderson & Garven, 1987; Machel, 1989; Shelton et al., 2009).

Metallogenetic model

Taking into consideration all the data discussed above, we propose the following scenario for the basin evolution (Fig. 14). The basinal brines were formed as a result of the evolution of the sedimentary basin (Hanor, 1979; Garven & Raffensperger, 1997; Pirajno, 2009). During compaction, connate waters trapped in the sediments were released and subjected to overpressuring, with the load of the overlying sediments, and increase in temperature, and their composition was modified via pressure dissolution of minerals at grain-to-grain boundaries. In addition, the regional compressional regime (Torgersen et al.,

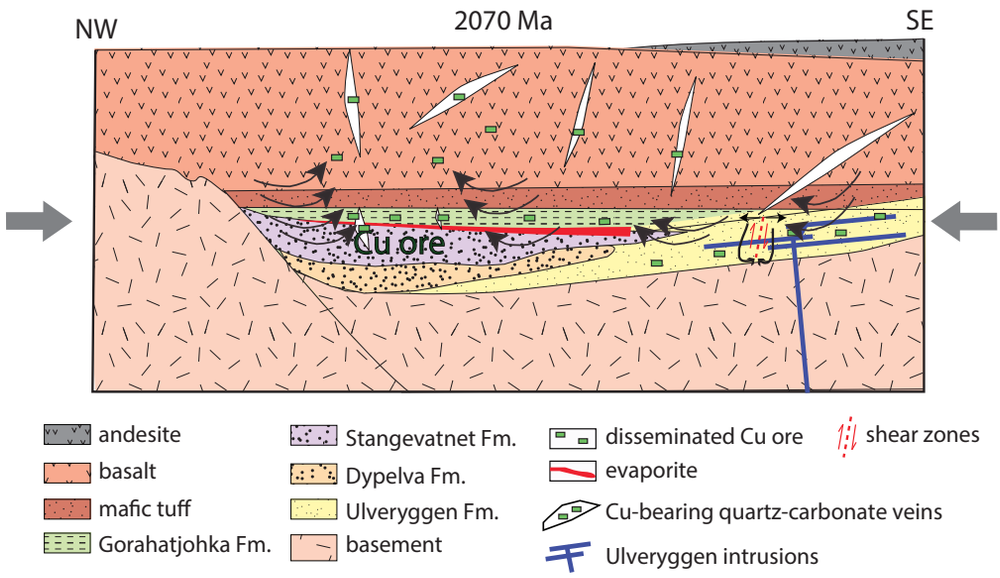

Figure 14. Inferred model for the evolution of the basin and metal-bearing fluids in the Nussir and Ulveryggen deposits. During the regional compressional event at c. 2.07 Ga (Torgersen et al., 2015a), fluids circulated in the basin and gradually consumed presently not preserved evaporates. The brines contained dissolved bicarbonate and, perhaps, Ca and Mg ions acquired with dissolution of the host dolostone rocks, in addition to chlorine and sulphate derived from evaporites. High brine temperature (>300°C), low pH, and high Cl content favoured leaching of base metals, including Cu, from host mafic volcanics, alkaline mafic intrusions, and Ulveryggen redbeds (for further discussion, see main text). The basinal brines contained Ba, Ca, Cl, Cu, Fe, K, Mg, Mn, Na, Ni, S, Si, and Ti. Organic matter in host dolostones (Gorahatjohka Formation) helped to sustain the reduction front at which metal-bearing brines precipitated mineralisation. Due to the brittle behaviour of dolostones and volcanic rocks, mineralised quartz-carbonate veins formed in these lithologies at the Nussir deposit. In contrast, highly porous sandstones, siltstones, and conglomerates at the Ulveryggen deposit resulted in the disseminated and fault-controlled quartz-associated mineralization (Sandstad et al., 2007). Small arrows schematically show movement of the brines. Modified from Sandstad et al. (2007) and Torgersen et al. (2015a).

2015a) increased the pressure and temperature in the buried basin, and further advanced dehydration reactions. The evolved fluids were forced to circulate convectively and along shear zones through the host mafic volcanic and siliciclastic rocks, sulphate evaporites, alkaline mafic intrusions and carbonates. Key factors in formation of the basinal brines were thus deep burial of the sedimentary succession and compression during the c. 2.07 Ga orogenic event (Torgerssen et al., 2015a).

The presence of several fluid-inclusion types and generations as well as a wide range of homogenisation temperatures indicate a long history of fluid circulation in the basin. The fluid inclusions reflect a progressive evolution of the fluids (Figs. 13 & 15). Type 1 FIs have a very wide range of homogenisation temperatures, overlapping with that for the Types 2 and 3 FIs. The types 2 and 3 FIs indicate brines with salinities as high as 36 wt.% NaCl equiv., which is only possible to achieve via evaporite dissolution, assuming that there was no input of magmatic fluids. Evaporites commonly develop on carbonate platforms (e.g., Warren, 1999), and the presence of evaporites is an important factor for formation of the copper stratiform sedimentary deposits (Pirajno, 2009). In the Repparfjord basin that contains mafic volcanic, siliciclastic and carbonate rocks, connate waters must have circulated through and dissolved an evaporite sequence, progressively increasing their metal mobilisation potential. Dissolved salts and sulphate are necessary to transport metals, including Cu, as metal-carrying complexes with chlorine, sulphate and sulphide to the redox front or shallow level in the basin, where cooling and reduction result in metal precipitation. The brines are also efficient in leaching Cu and forming mobile $CuCl_2$ complexes (Rose, 1976), and dissolved sulphate in these brines further helps to trap metals as sulphides at the reduction front with sulphate reduction. In order to generate a sulphide

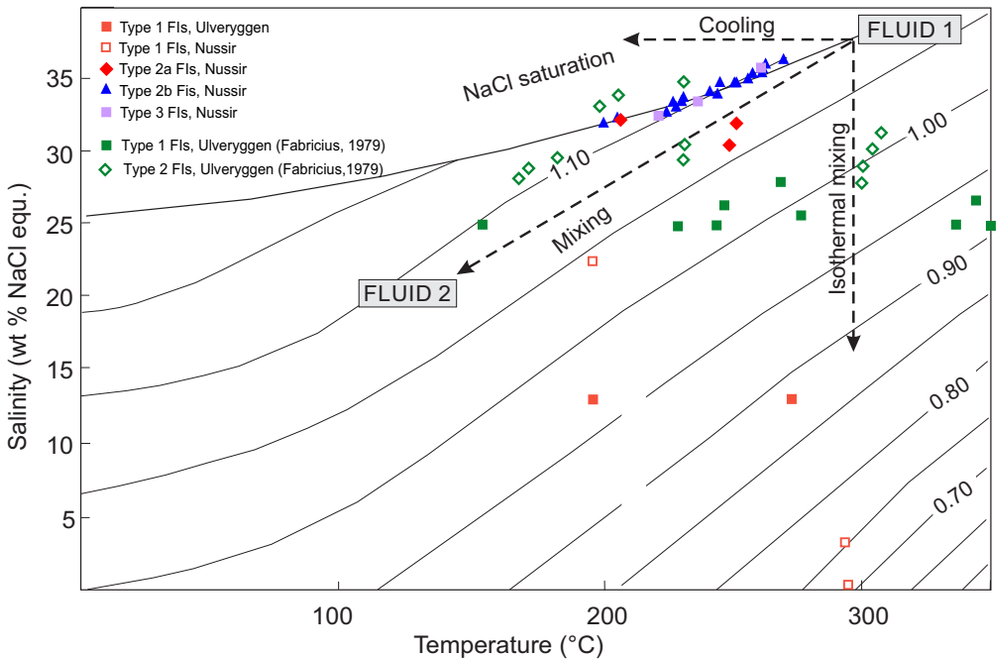

Figure 15. Relationship between the homogenisation temperature and salinity for analysed fluid inclusions. Isopleths of equal density (in g/cm³) are shown. Isothermal mixing trend implies mixing of two fluids with different salinities, but similar temperatures. Only a few inclusions show this trend. The Types 2b and 3 FIs plot along the 1.10 g/cm³ isopleth, just at the border with the NaCl saturation area and demonstrate a trend of gradual cooling.

deposit, large amounts of dissolved sulphate should be transported with the brine to the precipitation site within the basin. Therefore, dissolution of gypsum or anhydrite in the subsurface was necessary in the Repparfjord Tectonic Window to form the Nussir and Ulveryggen deposits. Dissolution of dolostones at this stage contributed Ca and Mg to basinal waters, resulting in calcite precipitation in veins, which are commonly observed in the sequence. Notably, mineralisation of the Nussir deposit is predominantly hosted in quartz-calcite veins.

Another critical factor in generating the Nussir–Ulveryggen mineralisation system was the source of metals and oxidising redox conditions necessary to transport them. Relevant to this, braided fluvial deposits of the Ulveryggen deposit could have been redbeds and if so provided metals and maintained oxidising conditions necessary for their mobilisation. The basinal brines that circulated through conglomerate and sandstone redbeds leached metals and were oxidised. Mafic volcanics and alkaline mafic intrusions could have been an additional source for base metals. Basinal brines delivered metals to the shallow levels in the basin, where brines were cooled and reduced, and metals were precipitated as sulphides in a disseminated form in the metasedimentary rocks of the Ulveryggen deposit and in quartz-carbonate veins in the metadolostones of the Nussir deposit, where organic matter sustained a reduction front.

Conclusions

The early Palaeoproterozoic Nussir and Ulveryggen sediment-hosted Cu deposits were formed by the basinal, moderately to highly saline brines that transported Cu and Fe in metal-bearing chlorine complexes in the aftermath of the Great Oxidation Event.

Both deposits were hydrothermally altered, and volcanic rocks of the volcano-sedimentary sequence hosting the Nussir deposit could be a potential metal source. The metaconglomerates and metasandstones of the Ulveryggen deposit might represent metamorphosed redbeds. Cu mineralisation is linked with carbonatisation in the volcano-sedimentary succession and interaction with saline brines.

The presence of both primary and secondary fluid inclusions and similar compositions of their decrepitated evaporite mounts suggest multiple remobilisation events involving metalliferous fluids. Combined with the previously published Re–Os dates, our data suggest a multistage mineralisation process that started shortly after deposition of the sediments and continued until the very late stage of the Svecofennian Orogeny.

The high salinity of the basinal fluids suggests involvement of evaporites that are no longer present. The circulated basinal brines had high ionic strength with Na, Mg, Mn, Ba and Ca enrichments. The temperature of the metal-bearing fluids was 330 to 340°C and the pressure was 1.1 to 2.7 kbars, which constrains the maximum burial depth to approximately 3.4–9 km, consistent with greenschist-facies metamorphism.

Overlapping $\delta^{13}C$ and $\delta^{18}O$ values for host carbonates and carbonates in the quartz-carbonate veins suggest a closed, rock-buffered system with little to no carbon added from magmatic, hydrothermal and organic sources. Metal-bearing brines must therefore have been in equilibrium with the host carbonates.

Acknowledgements. The authors would like to thank Troms Fylkeskommune and SINTEF for financing this research through a Ph.D. project for the first author (RDA12/167). Participation of AB was made possible with the funding from the NSERC Discovery and Accelerator grants. We would like to express our gratitude to the former and current staff of Nussir AS and Øystein Rushfeld for supporting us on field trips and providing us with access to the samples. Special thanks to Margarita Kim (The Institute of Geology and Geophysics of the Republic of Uzbekistan), Muriel Marie Laure Erambert (University of Oslo), and laboratory staff of the UiT for timely help with sample preparation and analysis. Thanks also to Dr.C. Shackleton for proofreading the manuscript and English language corrections

References

Anderson, G.M. & Garven, G. 1987: Sulfate-sulfide-carbonate associations in Mississippi Valley-type lead-zinc deposits. *Economic Geology 82*, 482–88. https://doi.org/10.2113/gsecongeo.82.2.482.

Bakker, R.J. 2003: Fluids, package of computer programs for fluid inclusion studies. *Chemical Geology 194*, 3–23. https://doi.org/10.1016/S0009-2541(02)00268-1.

Bakker, R.J. & Brown, P.E. 2003: Computer modelling in fluid inclusion research. In Samson, I., Anderson, A. & Marshall, D. (eds.): *Fluid Inclusions: Analysis and Interpretation.* Mineralogical Association of Canada 32, pp. 175–212.

Bankole, O.M., El Albani, A., Meunier, A., Rouxel, O.J., Gauthier-Lafaye, F. & Bekker, A. 2016: Origin of red beds in the Paleoproterozoic Franceville Basin, Gabon, and implications for sandstone-hosted uranium mineralization. *American Journal of Science 316,* 839–872. https://doi.org/10.2475/09.2016.02.

Banner, J.L. & Hanson, G.N. 1990: Calculation of simultaneous isotopic and trace element variations during water-rock interaction with applications to carbonate diagenesis. *Geochimica et Cosmochimica Acta 54,* 3123–3137. https://doi.org/10.1016/0016-7037(90)90128-8.

Bekker, A., Karhu, J.A. & Kaufman, A.J. 2006: Carbon isotope record for the onset of the Lomagundi carbon isotope excursion in the Great Lakes area, North America. *Precambrian Research 148,* 145–180. https://doi.org/10.1016/j.precamres.2006.03.008.

Bekker, A. & Holland, H.D. 2012: Oxygen overshoot and recovery during the early Paleoproterozoic. *Earth and Planetary Science Letters 317–318,* 295–304. https://doi.org/10.1016/j.epsl.2011.12.012.

Bekker, A. 2015: Great Oxydation Event. In Gargaud, M., Irvine, W.M., Amils, R., CleavesII, H.J., Pinti, D.L., Quintanilla, J.C., Rouan, D., Spohn, T., Tirard, S. & Viso, M. (eds.): *Encyclopedia of Astrology*, Springr, Berlin, Heidelberg. https://doi.org/10.1007/978-3-662-44185-5_1752.

Bennett, D.G. & Barker, A.J. 1992: High salinity fluids: the result of retrograde metamorphism in thrust zones. *Geochimica et Cosmochimica Acta 56,* 81–95. https://doi.org/10.1016/0016-7037(92)90118-3.

Bingen, B., Solli, A., Viola, G., Torgersen, E., Sandstad, J.S., Whitehouse, M.J., Røhr, T.S., Ganerød, M. & Nasuti, A. 2015: Geochronology of the Palaeoproterozoic Kautokeino Greenstone Belt, Finnmark, Norway: Tectonic implications in a Fennoscandia context. *Norwegian Journal of Geology 95,* 365–396. https://doi.org/10.17850/njg95-3-09.

Bodnar, R.J. 1993: Revised equation and table for determining the freezing point depression of H2O–NaCl solutions. *Geochimica et Cosmochimica 57*, 683–684. https://doi.org/10.1016/0016-7037(93)90378-A.

Bodnar, R.J. & Vityk, M.O. 1994: Interpretation of microthermometric data for H2O–NaCl fluid inclusions. In De Vivo, B. & Frezzotti, M.L. (eds.): *Fluid Inclusions in Minerals, Methods and Applications,* pub. by Virginia Tech, Blacksburg, VA, pp. 117–130.

Bogdanova, S., Gorbatschev, R., Skridlaite, G., Soesoo, A., Taran, L. & Kurlovich, D. 2015: Trans-Baltic Palaeoproterozoic correlations towards the reconstruction of supercontinent Columbia/Nuna. *Precambrian Research 259*, 5–33. https://doi.org/10.1016/j.precamres.2014.11.023.

Bogdanova, S.V., Gorbatschev, R. & Garetsky, R.G. 2016: Europe|East European Craton. *In Reference Module in Earth Systems and Environmental Sciences,* Elsevier, pp. 1–18. https://doi.org/10.1016/B978-0-12-409548-9.10020-X.

Brems, D., Muchez, Ph., Sikazwe, O. & Mukumba, W. 2009: Metallogenesis of the Nkana copper-cobalt South Orebody, Zambia. *Journal of African Earth Sciences 55,* 185–196. https://doi.org/10.1016/j.jafrearsci.2009.04.003.

Brown, A.C. 1971: Zoning in the White Pine copper deposit, Ontogon County, Michigan. *Economic Geology 66,* 543–573. https://doi.org/10.2113/gsecongeo.66.4.543.

Brown, A.C. 1984: Alternative sources of metals for stratiform copper deposits. *Precambrian Research 25,* 61–74. https://doi.org/10.1016/0301-9268(84)90024-X.
Brown, A.C. 1992: Sediment-hosted stratiform copper deposits. *Geoscience Canada 19,* 125–141.

Cailteux, J.L.H., Kampunzu, A.B., Lerouge, C., Kaputo, A.K. & Milesi, J.P. 2005: Genesis of sediment-hosted stratiform copper-cobalt deposits, Central African Copperbelt. *Journal of African Earth Sciences 42,* 134–158. https://doi.org/10.1016/j.jafrearsci.2005.08.001.

Carmichael, I.S.E. & Ghiorso, M.S. 1986: Oxidation-reduction relations in basic magma: a case for homogeneous equilibria. *Earth and Planetary Science Letters 78,* 200–210.
https://doi.org/10.1016/0012-821X(86)90061-0.

Chartrand, F.M. & Brown, A.C. 1985: The diagenetic origin of stratiform copper mineralization, Coates Lake, Redstone Copper Belt, N.W.T., Canada. *Economic Geology 80,* 325–343.
https://doi.org/10.2113/gsecongeo.80.2.325.

Corfu, F., Roberts, R.J., Torsvik, T.H., Ashwal, L.D. & Ramsay, D.M. 2007: Peri-Gondwanan elements in the Caledonian Nappes of Finnmark, Northern Norway: Implications for the paleogeographic framework of the Scandinavian Caledonides. *American Journal of Science 307*, 434–458.
https://doi.org/10.2475/02.2007.05.

Cox, D.P., Lindsey, D.A., Singer, D.A., Moring, B.C. & Diggles, M.F. 2007: Sediment-hosted copper deposits of the world: deposits models and database. U.S. Geological Survey Open-File Report 03-107, version 1.3. http://pubs.usgs.gov/of/2003/of03-107/ (accessed 31.08.2020).

Dewaele, S., Muchez, Ph., Vets, J., Fernandez-Alonzo, M. & Tack, L. 2006: Multiphase origin of the Cu–Co ore deposits in the western part of the Lufilian fold-and-thrust belt, Katanga (Democratic Republic of Congo). *Journal of African Earth Sciences 46*, 455–469. https://doi.org/10.1016/j.jafrearsci.2006.08.002.

Doe, B.R. 1994: Zinc, copper, and lead in mid-ocean ridge basalts and the source rock control on Zn/Pb in ocean-ridge hydrothermal deposits. *Geochimica et Cosmochimica Acta 58*, 2215–2223.
https://doi.org/10.1016/0016-7037(94)90006-X.

El Desouky, H.A., Muchez, Ph. & Cailteux, J. 2009: Two Cu–Co sulfide phases and contrasting fluid systems in the Katanga Copperbelt, Democratic Republic of Congo. *Ore Geology Reviews 36,* 315–332.
https://doi.org/10.1016/j.oregeorev.2009.07.003.

Engel, A.E.J., Engel, C.G. & Havens, R.G. 1965: Chemical characteristics of oceanic basalts and the upper mantle. *Geological Society of America Bulletin 76,* 719–734.
https://doi.org/10.1130/0016-7606(1965)76[719:CCOOBA]2.0.CO;2.

Eriksson, P.G. & Cheney, E.S. 1992: Evidence for the transition to an oxygen-rich atmosphere during the evolution of red beds in the Lower Proterozoic sequences of southern Africa. *Precambrian Research 54,* 257–269. https://doi.org/10.1016/0301-9268(92)90073-W.

Fabricius, J. 1979: Kobberforekomsten på Ulveryggen, Finnmark, Norge. *Dansk Geologisk Forening. Årsskrift for 1979*, 107–110.

Gablina, I.F. 1990: Mineralogical-geochemical criteria for identifying red-bed formations in metamorphic strata of the Precambrian in connection with copper content. *Lithology and Mineral Resources 3,* 95–109 [in Russian].

Gablina, I.F. & Malinovsky, Y.M. 2008: Periodicity of copper accumulation in the Earth's sedimentary shell. *Lithology and Mineral Resources 43,* 155–173. https://doi.org/10.1134/S0024490208020041.

Gale, A., Dalton, C.A., Langmuir, C.H., Su, Y. & Schilling, J.G. 2013: The mean composition of ocean ridge basalts. *Geochemistry, Geophysics, Geosystems 14*, 489–518. https://doi.org/10.1029/2012GC004334.

Garven, G. & Raffensperger, J.P. 1997: Hydrology and geochemistry of ore genesis in sedimentary basins. *In* Barnes, H.L. (ed.): *Geochemistry of ore deposits.* John Wiley & Sons, New York, pp. 146–165.

Gee, D.G., Fossen, H., Henriksen, N. & Higgins, A.K. 2008: From the early Paleozoic platforms of Baltica and Laurentia to the Caledonide orogen of Scandinavia and Greenland. *Episodes 31*, 44–51. https://doi.org/10.18814/epiiugs/2008/v31i1/007.

Grant, J.A. 1986: The isocon diagram; a simple solution to Gresens' equation for metasomatic alteration. *Economic Geology 81,* 1976–1982. https://doi.org/10.2113/gsecongeo.81.8.1976.

Grant, J.A. 2005: Isocon analysis: A brief review of the method and applications. *Physics and Chemistry of the Earth 30,* 997–1004. https://doi.org/10.1016/j.pce.2004.11.003.

Hanor, J.S. 1979: The sedimentary genesis of hydrothermal fluids. In Barnes, H.L. (ed.) *Geochemisty of Hydrothermal ore deposits*. John Wiley & Sons, New York, pp. 137–172.

Heijlen, W., Banks, D.A., Muchez, Ph., Stensgard, B.M. & Yardley, B.W.D. 2008: The nature of mineralizing fluids of the Kipushi Zn–Co–Cu deposit, Katanga, Democratic Republic of Congo: quantitative fluid inclusion analysis using lasera ablation ICP-MS and bulk crush-leach methods. *Economic Geology 103,* 1459–1482. https://doi.org/10.2113/gsecongeo.103.7.1459.

Hitzman, M., Kirkham, R., Broughton, D., Thorson, J. & Selley, D. 2005: The sediment-hosted stratiform copper ore system. *Economic Geology 100th Anniversary Vol.*, 609–642. https://doi.org/10.5382/AV100.19.

Hitzman, M.W., Selley, D. & Bull, S. 2010: Formation of sedimentary rock-hosted stratiform copper deposits through Earth history. *Economic Geology 105,* 627–639. https://doi.org/10.2113/gsecongeo.105.3.627.

Hutchison, M.N. & Scott, S.D. 1981: Sphalerite geobarometry in the Cu–Fe–Zn–S system. *Economic Geology 76*, 143–153. https://doi.org/10.2113/gsecongeo.76.1.143.

Jensen, P.A. 1996: *The Altenes and Repparfjord tectonic windows, Finnmark, northern Norway: Remnants of a Palaeoproterozoic Andean-type plate margin at the rim of the Baltic Shield.* PhD thesis, University of Tromsø, 120 pp.

Jiang, Yu., Niu, H., Bao, Zh., Shan, Q., Yang, W. & Yan, Sh. 2014: Fluid evolution of the Paleoproterozoic Hujiayu copper deposit in the Zhongtiaoshan region: evidence from fluid inclusions and carbon-oxygen isotopes. *Precambrian Research 255,* 734–747. https://doi.org/10.1016/j.precamres.2014.08.007.

Keith, J.D., Whitney, J.A., Hattori, K., Ballantyne, G.H., Christiansen, E.H., Barr, D.L., Cannan, T.M. & Hook, C.J. 1997: The role of magmatic sulphides and mafic alkaline magmas in the Bingham and Tintic Mining Districts, Utah. *Journal of Petrology 38,* 1679–1690. https://doi.org/10.1093/petroj/38.12.1679.

Kirkham, R.V. 1989: Distribution, settings, and genesis of sediment-hosted stratiform copper deposits. In Boyle, R.W., Brown, A.C., Jefferson, C.W., Jowett, E.C. & Kirkham, R.V. (eds.): *Sediment-hosted stratiform copper deposits,* Geological Association of Canada Special Paper 36, pp. 3–38.

Kirkland, C.L., Daly, J.S. & Whitehouse, M.J. 2006: Granitic magmatism of Grenvillian and late Neoproterozoic age in Finnmark, Arctic Norway—Constraining pre-Scandian deformation in the Kalak Nappe Complex. *Precambrian Research 145,* 24–52. https://doi.org/10.1016/j.precamres.2005.11.012.

Kontak, D.J. 2004: Analysis of evaporate mounds as a complement to fluid-inclusion thermometric data: case studies from granitic environments in Nova Scotia and Peru. *Canadian Mineralogist 42,* 1315–1329. https://doi.org/10.2113/gscanmin.42.5.1315.

Machel, H.G. 1989: Relationships between sulphate reduction and oxidation of organic compounds to carbonate diagenesis, hydrocarbon accumulations, salt domes, and metal sulphide deposits. *Carbonates and Evaporites 4*, 137–161. https://doi.org/10.1007/BF03175104.

Master, S., Bekker, A. & Hofmann, A. 2010: A review of the stratigraphy and geological setting of the Palaeoproterozoic Magondi Supergroup, Zimbabwe - type locality for the “Lomagundi” carbon isotope excursion. *Precambrian Research 182,* 254–273. https://doi.org/10.1016/j.precamres.2010.08.013.

Matthews, A. 1976: Magnetite formation by the reduction of hematite with iron under hydrothermal conditions. *American Mineralogist 61,* 927–932.

Melezhik, V.A. & Fallick, A.E. 1996: A widespread positive δ13Ccarb anomaly at around 2.33–2.06 Ga on the Fennoscandian Shield: a paradox? *Terra Nova 8,* 141–157. https://doi.org/10.1111/j.1365-3121.1996.tb00738.x.

Melezhik, V.A., Bingen, B., Sandstad, J.S., Pokrovsky, B.G., Solli, A. & Fallick, A.E. 2015: Sedimentary-volcanic successions of the Alta–Kvænangen Tectonic Window in the northern Norwegian Caledonides: Multiple constraints on deposition and correlation with complexes on the Fennoscandian Shield. *Norwegian Journal of Geology 95*, 245–284. https://doi.org/10.17850/njg95-3-01.

Mun, Y. 2013: *The Nussir copper deposit: petrology, mineralogy, geochemistry and distribution of ore mineralization*. MSc thesis. University of Tromsø, 54 pp.

Nasuti, A., Roberts, D., Dumais, M.-A., Ofstad, F., Hyvönen, E., Stampolidis, A. & Rodionov, A. 2015: New high-resolution aeromagnetic and radiometric surveys in Finnmark and North Troms: linking anomaly patterns to bedrock geology and structure. *Norwegian Journal of Geology 95,* 217–243. https://doi.org/10.17850/njg95-3-10.

Nordgulen, Ø. & Andresen, A. 2008: The Precambrian. In Ramberg, I.B., Bryhni, I., Nøttvedt, A. & Rangnes, K. (eds.): *The making of land – geology of Norway,* Norsk Geologisk Forening, Trondheim, pp. 58–119.

Nussir ASA 2019: Official grades from Nussir ASA. http://www.nussir.no/en_projec_nussir.php (accessed 20.06.2019).

Perelló, J., Clifford, J.A., Creaser, R.A. & Valencia, V.A. 2015: An example of synorogenic sediment-hosted copper Mineralization: geologic and geochronologic evidence from the Paleoproterozoic Nussir deposit, Finnmark, Arctic Norway. *Economic Geology 110,* 677–689. https://doi.org/10.2113/econgeo.110.3.677.

Pharaoh, T.C. 1985: Volcanic and Geochemical Stratigraphy of the Nussir Group of Arctic Norway – an Early Proterozoic Greenstone Suite. *Journal of the Geological Society, London 142*, 259–278. *https://doi.org/10.1144/gsjgs.142.2.0259.*

Pharaoh, T.C., MacIntyre, R.M. & Ramsay, D.M. 1982: K–Ar age determination on the Raipas suite in the Komagfjord Window, northern Norway. *Norwegian Journal of Geology 62*, 51–57.

Pharaoh, T.C., Ramsay, D. & Jansen, Ø. 1983: Stratigraphy and structure of the northern part of the Repparfjord–Komagfjord window, Finnmark, Northern Norway. *Norges Geologiske Undersøkelse 377,* 1–45.

Pharaoh, T.C. & Brewer, T.S. 1990: Spatial and temporal diversity of early Proterozoic volcanic sequences – comparison between the Baltic and Laurentian shields. *Precambrian Research 47*, 169–189. https://doi.org/10.1016/0301-9268(90)90037-Q.

Pharaoh, T.C. & Pearce, J.A. 1984: Geochemical evidence for the geotectonic setting of early Proterozoic metavolcanic sequences in Lapland. Precambrian Research 25, 283–308. https://doi.org/10.1016/0301-9268(84)90037-8.

Pirajno, F. 2009: *Hydrothermal processes and mineral systems.* Springer Science, Business Media B.V., 1249 pp. https://doi.org/10.1007/978-1-4020-8613-7.

Planavsky, N.J., Bekker, A., Hofmann, A., Owens, J.D. & Lyons, T.W. 2012: Sulfur record of rising and falling marine oxygen and sulfate levels during the Lomagundi event. *Proceedings of the National Academy of Sciences of the United States of America 109,* 18300–18305. https://doi.org/10.1073/pnas.1120387109.

Reitan, P.H. 1963: The geology of the Komagfjord tectonic window of the Raipas suite, Finnmark, Norway. *Norges Geologiske Undersøkelse 221*, 1–71.

Ripley, E.M., Lambert, M.W. & Berendsen, P. 1980: Mineralogy and paragenesis of Red-Bed copper mineralization in the Lower Permian of South Central Kansas. *Economic Geology 75,* 722–729. https://doi.org/10.2113/gsecongeo.75.5.722.

Roedder, E. 1984: *Fluid inclusion*. Reviews in mineralogy 12, 646 pp. https://doi.org/10.1515/9781501508271.

Rose, A.W. 1976: The effect of cuprous chloride complexes in the origin of red-bed copper and related deposits. Economic Geology 71, 1036–1048. https://doi.org/10.2113/gsecongeo.71.6.1036.

Sandstad, J.S. 2010: Microscope and SEM (scanning electron microscope) investigations of thin sections from the Nussir copper deposit. *NGU Report 2010.025,* 55 pp.

Sandstad, J.S., Viola, G. & Nilsson, L.P. 2007: Reconnaissance structural geological mapping and field XRF-analyses of the Ulveryggen copper deposit, Finnmark, Norway. *NGU Report 2007.064,* 16 pp.

Schröder, S., Bekker, A., Beukes, N.J., Strauss, H. & Van Niekerk, H.S. 2008: Rise in seawater sulphate concentration associated with the Paleoproterozoic positive carbon isotope excursion: evidence from sulphate evaporites in the ~ 2.2–2.1 Gyr shallow-marine Lucknow Formation, South Africa. Terra Nova 20, 108–117. https://doi.org/10.1111/j.1365-3121.2008.00795.x.

Selley, D., Broughton, D., Scott, R., Hitzman, M., Bull, S., Large, R., McGoldrick, P., Croaker, M., Pollington, N. & Barra, F. 2005: A new look at the Geology of the Zambian Copperbelt. Economic Geology 100th *Anniversary Volume*, 965–1000. https://doi.org/10.5382/AV100.29.

Seward, T.M., Williams-Jones, A. & Migdisov, A. 2013: The chemistry of metal transport and deposition by ore-forming hydrothermal fluids. In Holland, H.D. & Turekian K.K. (eds.): *Treatise on Geochemistry.* Elsevier, 2nd Edition, pp. 29–57. https://doi.org/10.1016/B978-0-08-095975-7.01102-5.

Shelton, K.L., Gregg, J.M., & Johnson, A.W. 2009: Replacement dolomites and ore sulphides as recorders of multiple fluids and fluid sources in the Southeast Missouri Mississipi Valley-Type District: halogen-$^{87}Sr/^{86}Sr$-$\delta^{18}O$-$\delta^{34}S$ systematics in the Bonneterre Dolomite. *Economic Geology 104,* 733–748. https://doi.org/10.2113/gsecongeo.104.5.733.

Siedlecka, A., Krill, A.G., Often, M., Sandstad, J.S., Solli, A., Iversen, E. & Lieungh, B. 1985: Litho-stratigraphy and correlation of the Archaean and Early Proterozoic rocks of Finnmarksvidda and the Sørvaranger district. *Norges Geologiske Undersøkelse Bulletin 403*, 7–36.

Sillitoe, R.H., Perelló, J. & Carcía, A. 2010: Sulfide-bearing veinlets throughout the stratiform mineralization of the Central African Copperbelt: temporal and genetic implications. *Economic Geology 105*, 1361–1368. https://doi.org/10.2113/econgeo.105.8.1361.

Singer, D.A. 1995: World class base and precious metal deposits – a quantitative analysis. *Economic Geology 90*, 88–104. https://doi.org/10.2113/gsecongeo.90.1.88.

Stakes, D.S. & O'Neil, J.R. 1982: Mineralogy and stable isotope geochemistry of hydrothermally altered oceanic rocks. *Earth and Planetary Science Letters 57,* 285–304. https://doi.org/10.1016/0012-821X(82)90151-0.

Stribrny, B. 1985: *The conglomerate-hosted Repparfjord copper ore deposit, Finnmark, Norway.* Monograph Series on Mineral Deposits 24. Gebrüder Borntraeger, Berlin, Stuttgart, 75 pp.

Torgersen, E. & Viola, G. 2014: Structural and temporal evolution of a reactivated brittle-ductile fault – Part I: Fault architecture, strain localization mechanisms and deformation history. *Earth and Planetary Science Letters 407*, 205–220. https://doi.org/10.1016/j.epsl.2014.09.019.

Torgersen, E., Viola, G., Zwingmann, H. & Harris, C. 2014: Structural and temporal evolution of a reactivated brittle-ductile fault – Part II: Timing of fault initiation and reactivation by K–Ar dating of synkinematic illite/muscovite. *Earth and Planetary Science Letters 407*, 221–233. https://doi.org/10.1016/j.epsl.2014.09.031.

Torgersen, E., Viola, G. & Sandstad, J.S. 2015a: Revised structure and stratigraphy of the northwestern Repparfjord Tectonic Window, Northern Norway. *Norwegian Journal of Geology 95*, 397–421. https://doi.org/10.17850/njg95-3-06.

Torgersen, E., Viola, G., Sandstad, J.S., Stein, H., Zwingmann, H. & Hannah, J. 2015b: Effects of frictional-viscous oscillations and fluid flow events on the structural evolution and Re–Os pyrite-chalcopyrite systematics of Cu-rich carbonate veins in northern Norway. *Tectonophysics 659,* 70–90. https://doi.org/10.1016/j.tecto.2015.07.029.

Torske, T. & Bergh, S.G. 2004: The Caravarri Formation of the Kautokeino Greenstone Belt, Finnmark, North Norway. Palaeoproterozoic foreland basin succession. *Norges Geologiske Undersøkelse Bulletin 442*, 5–22.

Viola, G., Sandstad, J.S., Nilsson, L.P. & Heincke, B. 2008: Structural and ore geological studies in the northwestern part of the Repparfjord Window, Kvalsund, Finnmark, Norway. *NGU Report 2008.029*, 93 pp.

Warren, J. 1999: *Evaporites: their evolution and economics.* Blackwell Science, 438 pp.

Zhang, Y.-G. & Frantz, J.D. 1987: Determination of the homogenization temperatures and densities of supercritical fluids in the system NaCl–KCl–CaCl2–H2O using synthetic fluid inclusions. *Chemical Geology 64*, 335–350. https://doi.org/10.1016/0009-2541(87)90012-X.

Table 1. Whole-rock data for basaltic andesites and tuffs from the Nussir deposit. 'Mineralised' refers to rocks having Cu contents higher than the background value.

Table 2. Whole-rock data for carbonate-siliciclastic rocks from the Nussir deposit. 'Mineralised' refers to rocks having Cu contents higher than the background value.

Table 3. Whole-rock data for siliciclastic rocks from the Ulveryggen deposit. 'Mineralised' refers to rocks having Cu contents higher than the background value.

Table 4. Mineral chemistry of the selected ore minerals from the Nussir and Ulveryggen deposits.

Table 5. Chemical data for selected decrepitated evaporate mounds obtained with EDS detector (wt.%).

Table 6. Carbon and oxygen isotope composition of host dolomitic marble and ore-bearing carbonate veins.